J. Physiol. (1983), **344**, *pp.* 549–583
With 18 *text-figures*
Printed in Great Britain

A DESCRIPTION OF ACTIVATION AND CONDUCTION IN CALCIUM CHANNELS BASED ON TAIL AND TURN-ON CURRENT MEASUREMENTS IN THE SNAIL

BY A. M. BROWN, Y. TSUDA AND D. L. WILSON

From the Department of Physiology and Biophysics, University of Texas Medical Branch, Galveston, TX 77550, U.S.A.

(*Received 18 August 1982*)

SUMMARY

1. Turn-on of Ca currents, or activation, was compared with turn-off, or de-activation. The experiments were done on nerve cell bodies of *Helix aspersa* separated by dissection, voltage-clamped and internally perfused using a combined suction pipette–micro-electrode method. Ca currents were isolated by suppression of Na and K currents.

2. The turn-off or tail currents were large and fast; this required that the limitations of the voltage clamp be established. A second micro-electrode was inserted to determine temporal and spatial control of potential, and it was found that the cells were essentially equipotential within 60 μsec during the largest tail currents. Series resistance was < 5 kΩ as measured by a small-perturbation, pseudorandom noise-current signal and presented negligible error in the measurements.

3. Activation was complicated by the presence of asymmetry currents which required evaluation. This was done after Co replacement for Ca. The asymmetry currents were sufficiently small for their contribution to the tail currents to be ignored. Addition of Cd to Ca solutions could not be used since relatively large inward tail currents persisted in the presence of Cd.

4. Tail currents were fitted by sums of two or three exponentials; each was sensitive to Ca-channel blockers but only two were due to closure of Ca channels. The two faster components with time constants τ_F and τ_S, for fast and slow respectively, were produced by brief, 3·0 msec voltage pulses and were present in all cells. The third and slowest component with time constant τ_{VS}, for very slow, activated much more slowly and was not always present. The amplitudes of τ_F and τ_S were reduced by cooling and were increased when Ca was replaced by Ba extracellularly or when the external Ca concentration was increased. Hence, these components were due to closure of Ca channels.

5. The third component activated faster in Ba solution. When fully activated it had the same amplitude in either Ba or Ca solution despite the differences in amplitude of Ba and Ca currents during the voltage-clamp step. The amplitude of the third component was also not changed by increasing external Ca concentration; hence it was not due to closure of Ca channels. Cooling also had very little effect. The third component was abolished by Ca blockers, but it does not appear to be related

to previously described Ca-activated currents. It also does not appear to be related to the non-specific current, I_{NS}, as defined earlier (Brown, Morimoto, Tsuda & Wilson, 1981).

6. In cells without the slowest component, τ_F and τ_S remained unchanged as the duration of the voltage pulse was increased to 400 msec. The envelope of the tail current amplitudes had a similar time course to the current produced during the voltage-clamp step, namely an increase followed by a relatively slow decrease. The constancy of the two τ values excluded the occurrence of contaminating outward currents which may have developed with time and is good evidence for inactivation of Ca current.

7. In cells having only two components in the tail currents, turn-on was well described over most of the voltage range by an m^2 Hodgkin–Huxley activation process having time constants τ_m and $\tau_m/2$. However, the ratio τ_F/τ_S varied between 6 or 8 to 1 rather than the fixed 2 to 1 required by an m^2 model.

8. τ_S fell between the two time constants required to fit the turn-on and therefore probably reflected a time course which was a weighted sum of these two exponentials. τ_F had a different voltage dependence from τ_S. τ_F and τ_S could account for the delayed turn-on of I_{Ca} at depolarized potentials above zero mV, but τ_F was too small to account for the delay at less depolarized potentials.

9. From consideration of the turn-on and tail Ca currents at the same potential, it was found that at least three distinct exponentials were required to describe the total activation process. Two exponentials were required to fit turn-on, whereas a third, much faster exponential was revealed by turn-off. The fact that there were three exponentials in the system response indicates a minimum of four states in a transition state model of activation. The effect of cooling to slow turn-on with little effect on tail τ values was explained by making the leading forward rate constant of the four-state model more temperature-sensitive than the other rate constants.

10. The instantaneous current–voltage (I–V) curve was made up of the amplitudes associated with the fast and slow exponentials, denoted A_F and A_S, respectively. The instantaneous I–V curve was fitted by a modified constant field equation, and the dominant A_F component had the same shape. The slower component however had a constant amplitude at potentials below +10 mV. These results may help explain the different instantaneous I–V curves that have been described for the Ca channel.

11. An isochronal I–V was measured using the current at the end of 3 msec pulses, and this was in good agreement with an I–V curve which was constructed from an activation curve and an instantaneous I–V curve, both of which were obtained from tail current measurements.

INTRODUCTION

The turning-on, or activation, of Ca currents has been described for molluscan neurones in Hodgkin–Huxley (1952) terms using the activation variable, m, in powers of 1–5 ($m = 2$, Kostyuk, Krishtal, Pidoplichko & Shakhovalov, 1979 and Kostyuk, Krishtal & Pidoplichko, 1981; $m = 1$, Akaike, Lee & Brown, 1978; $m = 5$, Llinas, Steinberg & Walton, 1981). Recently Byerly & Hagiwara (1982) and Tsuda, Wilson & Brown (1982*a*) using snail neurones, and Fenwick, Marty & Neher (1982) using mammalian chromaffin ganglion cells have found a clear inconsistency with the

Hodgkin–Huxley model, namely that deactivation or turning-off of Ca tail currents has a component with a time constant that is much smaller than the activation time constants determined from the Hodgkin–Huxley model. Byerly & Hagiwara (1982) found three exponential components in the tail currents, only one of which they attributed to closure of Ca channels. Fenwick *et al.* (1982) came to a different conclusion: they found two components both of which were attributed to Ca channel closure.

Conduction in Ca channels based on tail currents has also been described in various ways. Saturation of the I–V curve at hyperpolarizing potentials was reported by Kostyuk *et al.* (1981) and Llinas *et al.* (1981), whereas a curvilinear relationship similar to a constant field prediction was reported by Fenwick *et al.* (1982).

In the present paper we have examined the total activation process using measurements of Ca tail and turn-on currents. Instantaneous conduction has been measured from the tail currents as well. Our results help to reconcile the differences that have been reported for activation and conduction and indicate that as a minimum, a four-state model is necessary to account for the total activation process.

METHODS

Preparation

The circumoesophageal ganglia were dissected from *Helix aspersa*, and the surrounding connective tissue was removed using fine tweezers and scissors. The ganglia were perfused continuously in normal extracellular snail Ringer solution (see *Solutions*) for about 15–20 min, a process which we have found helpful for the further removal of connective tissue. The neurones were then isolated by dissection alone. We selected neurones of 60–100 μm diameter because this size was large enough to accommodate our two-electrode voltage clamp, yet small enough to help ensure the spatial control of the voltage. The neurone was held to the suction pipette by gentle suction (Lee, Akaike & Brown, 1980) and the portion of membrane aspirated into the pipette was ruptured using an etched Pt–Ir wire; this step was found to be essential for satisfactory internal perfusion. The axon was then severed near the neurone (within 50 μm) by pinching it with fine forceps or cutting it with the tip of a broken micro-electrode. Upon cutting the axon, the voltage response to hyperpolarizing current pulses decreased by about 20%. In cases where the membrane impedance did not return to its original value in about 5–10 min indicating a 'healing over' of the neurone, the cell was discarded.

We required three additional criteria before an isolated cell was used. The action potential amplitude had to be at least 80 mV when measured with the suction pipette, and it had to remain constant during repetitive firing; the resting potential had to be about -50 mV; and after impalement with a separate micro-electrode the holding current required to keep the cell at -50 mV had to be $< 10^{-9}$ A. Cells which met these requirements had input resistances of about 5–10 MΩ; these values were comparable to values measured following the insertion of two micro-electrodes (Brown, Morimoto, Tsuda & Wilson, 1981). With these methods, successful isolations were obtained about 25–30% of the time.

We also tried to isolate cell bodies by exposure to trypsin in varying amounts (1%, 0·5% and 0·2% w/v) in normal Ringer solution for about 5–10 min at room temperature. The neurone was almost completely exposed before trypsin was applied. We found cells treated in this way had a high input resistance, characteristic of a good seal between the pipette and cell membrane. However, we found such cells to be fragile; the currents often ran down within 15–30 min following the commencement of internal perfusion. The Ca currents became small to insignificant and leakage resistance fell to very low levels.

Solutions and bath temperature

The following solutions were used. Normal extracellular Ringer solution (mM): NaCl, 85; KCl, 5; $CaCl_2$, 10; $MgCl_2$, 15; Tris Cl, 5; glucose, 5·5; pH 7·5 adjusted by Tris base. Normal intracellular

Ringer solution: K aspartate, 135; pH 7·3 adjusted by Tris base. For isolation of Ca currents, the extracellular solution (mM) was: Tris Cl, 35; tetraethylammonium (TEA) Cl, 50; CsCl, 5; 4-aminopyridine, 5; $MgCl_2$, 15; $CaCl_2$, 10; glucose, 5·5; pH 7·5 adjusted by Tris base. The intracellular solution was: Cs aspartate, 135; TEA OH, 10; pH 7·3 adjusted by Tris base or HEPES. EGTA, 0·1 mM, was added to the intracellular solution giving a Ca concentration of $4–6 \times 10^{-8}$ M as measured with a Ca-sensitive electrode using a Simon type of Ca exchanger. For studying Ba currents, extracellular $CaCl_2$ was replaced by $BaCl_2$. Ca currents were blocked by substituting $CoCl_2$ for $CaCl_2$. Cd was also used as a blocker and 1 mM-$CdCl_2$ was added to the solution in the presence of either $CaCl_2$ or $BaCl_2$. Bath temperature was monitored (Tele-Thermister, Hypodermic Temperature probe, Yellow Spring Instruments) and controlled by a cooling–heating device (Cambion Instruments). All but the cooling experiments were done at room temperature.

The suction pipette

Details of construction were given by Tsuda, Wilson & Brown (1982*b*) and Lee *et al.* (1980). At present we use 3 mm outer diameter (o.d.) Pyrex glass which is pulled to a shank length of about 4 mm. The glass is scored and broken at an o.d. of 50–60 μm and then fire-polished to give an inner diameter of about 15–20 μm. The same suction pipette can be used for many months if the tip is cleaned before and after each experiment.

Adequacy of internal perfusion

We assessed the adequacy of internal perfusion routinely using the following criteria. With a normal Ringer external solution present, we replaced the normal internal perfusate with the internal solution used to isolate the Ca current. During the ensuing 10–20 min of perfusion, prominent prolongation of action potential duration from a half-peak value of about 10 msec to 3–4 sec occurred. Then we changed the bath from normal Ringer solution to the external solution used for isolation of the Ca current; this provided no significant further change in the action potential and was a good test for satisfactory intracellular exchange. In contrast, when the internal perfusate was K rather than Cs aspartate, changing the extracellular solution produced large increases in the duration of the action potential. Next, a silver-painted, insulated glass micro-electrode filled with 3 M-CsCl and having a tip resistance of 1–2 MΩ was inserted into the cell. Voltage clamp was applied and in healthy cells a step to +20 mV was expected to produce an inward current of about 80–100 nA that peaked in about 3–4 msec at room temperature. The cell was pulsed at intervals of 5–10 sec for 30–60 min to determine whether the magnitude and time course of the inward current remained constant. When this was the case we proceeded with the experiment.

The voltage-clamp system

Fig. 1*A* is a schematic diagram of the experimental arrangement and the voltage-clamp circuit which includes the following improvements. A high-frequency op amp (Teledyne-Philbrick 1030) with a gain–band width product of 100 MHz was used as the voltage-clamp amplifier. As pointed out by Fishman (1982) a wide-band amplifier allows the voltage clamp to be used at higher frequencies with stability. The glass micro-electrodes for measuring membrane potential were painted with silver, insulated and driven with capacitance compensation. This resulted in a significant increase in the band width of the voltage measurement, and in several cases we measured the amplitude response of carefully painted and compensated micro-electrodes to be flat up to as much as 10 kHz, as described in the Appendix. The inlet and outlet tubing surrounding the suction electrode have been greatly shortened to reduce stray capacitances. Nevertheless, a measurement of the current in the bath was found to be necessary since there was significant capacitive shunting of the suction pipette apparatus to ground, as discussed in the Appendix; thus current measurements were made using a current-to-voltage converter circuit as shown in Fig. 1*A* and the bath electrode was a silver/silver chloride pellet. After application of voltage clamp the circuit was tuned in such a way that the full op amp gain was applied to the circuit, and the compensation capacitor was set at its minimum setting to obtain a damped voltage trace.

Time resolution and spatial control of the voltage clamp

As shown in Fig. 1*B*, the voltage-clamp pulse was complete in $\sim$ 30 μsec, and the capacitive transient decays in two phases, of which the large, fast phase subsides almost totally within 60 μsec. A slower phase of the relaxation, with amplitude around 5% of the fast phase, was also present

and has been reported by Byerly & Hagiwara (1982). Its nature is unknown although Byerly & Hagiwara (1982) have suggested a relationship to the piece of membrane aspirated in the suction pipette. Preliminary measurements indicate a constant phase angle in impedance measurements (see Appendix) similar to that observed in squid axon and this is consistent with such a capacitive transient (Cole, 1976). Over the voltage range examined, linearity of both capacitive current components was confirmed by scaling and overlaying hyperpolarizing responses. These linear

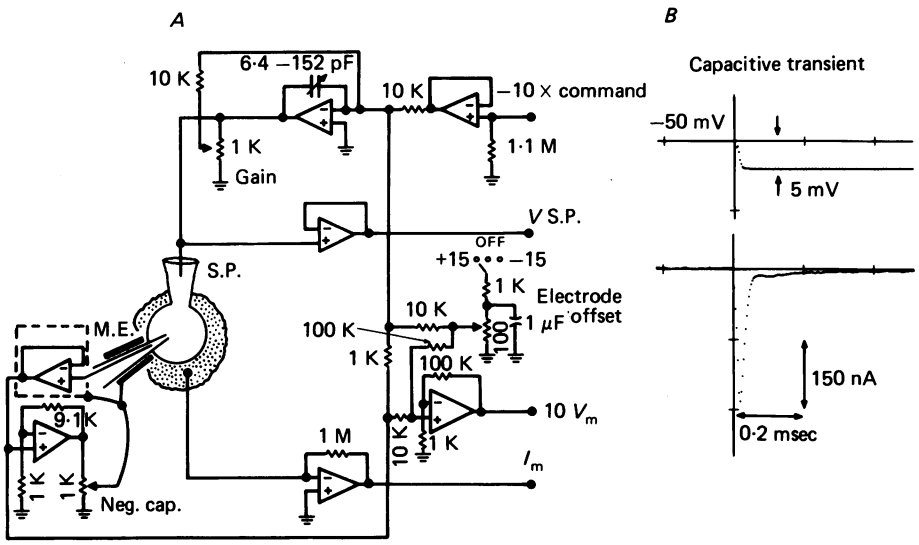

Fig. 1. *A*, diagram of the voltage-clamp system. A micro-electrode (M.E.) was used for voltage-sensing and a suction pipette (S.P.) was used for passing current and internal perfusion of the cell, and they are shown with a neurone immersed in a patch of fluid. The micro-electrode headstage was attached directly to the micro-electrode holder, and it and the micro-electrode shield were driven from the capacitance neutralization circuit. In addition to the circuit components shown here the design included other features such as a 'current pump' source, a 'model cell' circuit, and a circuit for testing the micro-electrode response. All op amps were of the LF356 type except the 'voltage-clamp amplifier' (the one with the variable capacitor) which was a Teledyne-Philbrick 1030. (Full circuit details are available upon request.) *B*, the capacitive transient for a subthreshold depolarizing pulse. The voltage trace shown has a rise time of ~ 25 μsec. There were two phases in the decay of the current, a faster one which was almost complete in 60 μsec and a slower, much smaller component which lasted over 0·5 msec.

capacitive components of the response were removed by summation of equal but opposite voltage-clamp pulses. The resulting sum of the voltage traces for hyperpolarizing and depolarizing voltage pulses was monitored, and the maximum deviation from a straight line was on the order of 0·03 mV. This indicates that the voltage pulses were symmetrical and there was no loss of control due to ion conduction.

The spatial control was examined using a second, silver-painted, insulated micro-electrode with negative capacitance compensation. This electrode was 'outside' the clamp circuit. The suction pipette and the two glass micro-electrodes were placed at three different points having a roughly triangular distribution about the cell. Conditions were imposed that placed the greatest stress on spatial control, namely control during tail currents produced by steps to potentials that activate I_{Ca} maximally. Fig. 2 shows the voltage differences between the two micro-electrodes ($V_1 - V_2$) at these times. The difference is around 3 mV within 30 μsec and less than 1 mV within 100 μsec. These results suggest that the internal resistance of the cell is small and the almost spherical neurone is adequately spatially clamped.

We measured the series resistance, R_S, by frequency domain, impedance measurements (Appendix). The results show that R_S is less than 5 kΩ. Initially all the voltage drop will occur across R_S when voltage steps are begun, but as Fig. 1 shows the capacitive current effects are much reduced within 60 μsec. Since R_S was so small, less than 0·05 % of the resting input impedance of the cell, the added complexity of R_S compensation was not found to be necessary.

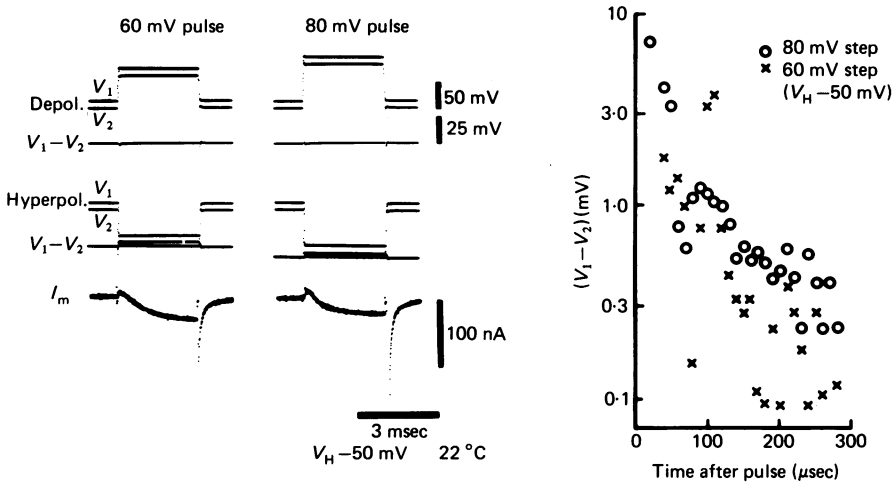

Fig. 2. Isopotentiality of cell body during voltage clamp. V_1 and V_2 are voltages measured by two different micro-electrodes, one of which was used in the voltage-clamp circuit as shown in Fig. 1. V_2 is displaced vertically with respect to V_1. Voltage steps shown were depolarizing of 60 and 80 mV; smaller steps gave much less difference between the two voltages. The difference in voltage between the two electrodes is displayed on both the left and right panels. The voltage difference in the diagram on the far right is displayed on a logarithmic scale and the voltage difference was less than 1 mV at 100 μsec. The currents shown result from summation of equal and opposite voltage pulses. Note that the current traces show an initial outward asymmetry current and the tail currents relax in two phases. Some of the initial data points in the tail currents have not reproduced in this Figure; the size of the initial tail currents are on the order of 200–300 nA.

Data analysis

Analog filtered data were digitized with sampling intervals as brief as 4 μsec per point using a Nicolet signal averager (Nicolet 1170). The averager allowed 1024, 2048, or 4096 data points, evenly spaced in time, to be digitized, stored on magnetic tape and subsequently transferred to a PDP-11/70 computer for detailed analysis. In almost all cases signal averaging of 5, 10 or 20 pulses was used to improve the signal-to-noise ratio. The data were fitted to products or sums of exponentials. For estimation of the parameters of the models, we used a Marquardt–Levenberg algorithm which allows rapid estimation and good noise insensitivity as compared to other methods (Thomasson & Clark, 1974). The sum of the squared error was minimized and typically several hundred equally weighted data points were used. We provided analytical expressions for the evaluation of the partial derivatives (Bevington, 1969). The parameter estimation routine was in a computer program which allowed for the rapid setting up of the data using cursors on a Tektronix 4010 terminal. Using the cursors one could set the boundaries for the data points to be fitted, the zero time for the function evaluations, and the zero current level. Convergence was usually quite good, and the stopping criteria used was normally a value of less than 10^{-5} for the percentage change in the sum of the squared error. In some cases, spline smoothing (deBoor, 1978) or a three-point smoothing filter was applied to the data to reduce noise present in the signal.

RESULTS

Asymmetry currents and the effects of Ca channel blockers

After isolation of Ca currents, we measured a fairly large initial outward current that has been interpreted as a Ca-channel gating current (Kostyuk, Krishtal & Pidoplichko, 1977, Kostyuk *et al.* 1979; Adams & Gage, 1977). We prefer the less specific term 'asymmetry current' (Hagiwara & Byerly, 1981; Brown, Akaike & Lee, 1979). We wished to correct for the asymmetry current in our experiments, since the

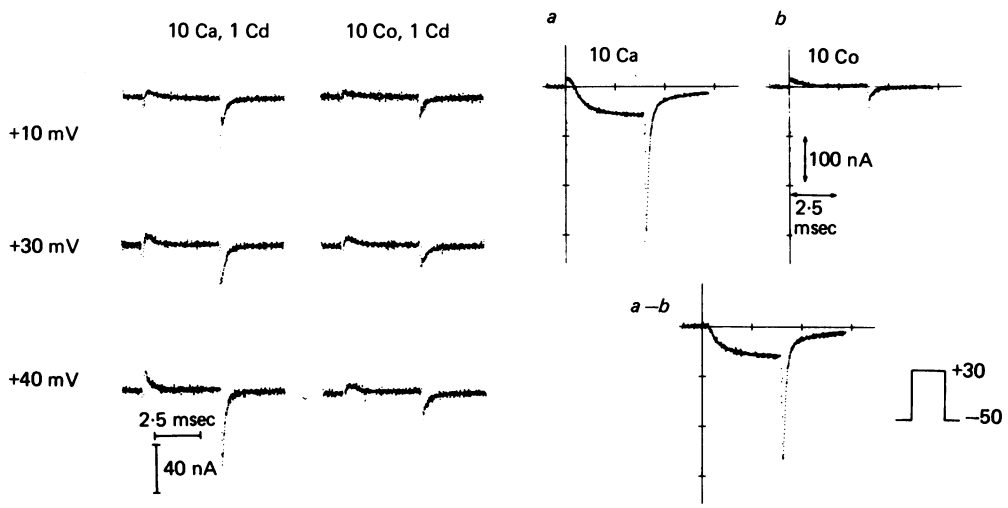

Fig. 3. Effects of Cd and Co ions on Ca tail currents. Left, currents were recorded at the potentials shown and were corrected for linear leakage and capacitive components by summation of ten hyperpolarizing and ten depolarizing pulses. In Cd, the voltage-dependent relief of block is seen in the tail currents, especially following the larger depolarizations. After Co replacement for Cd, the off-current was very much reduced. Right, in *a* and *b*, currents are shown before and after Co substitution for Ca. Note that in this cell there was a significant tail current evident at more than 3 msec following return to the holding potential. This cell would be classified as one having a slow component in the tail current relaxation. Note that the outward asymmetry current is eliminated when trace *b* is subtracted from trace *a*. Concentrations are in mM in this and subsequent Figures.

time course of ionic Ca current activation was to be evaluated. We thus examined the effects of two commonly used inorganic Ca-channel blockers, Cd and Co ions. Fig. 3 (right) shows that the tail currents as well as the current during the pulse were eliminated by Co substitution for Ca. Note that the tail current shown is relatively long lasting and that this cell is classified as having three tail current components (see later results). The Ca current remaining after the subtraction of the asymmetry obtained in Co is also shown. Fig. 3 (left) illustrates the effects of adding 1 mM-$CdCl_2$ to the Ca solution, and then replacing the Ca with Co. In Cd solutions there was no evidence of a net inward current during the voltage step and the initial outward asymmetry current remained unchanged. Unlike the current during the pulse, the tail currents were not totally suppressed. The amplitudes of both the slow and fast phases of the tail current were depressed almost equally by about 80%. The

integrated currents (Q) during the initial outward or ON asymmetry response were much smaller than the subsequent inward or OFF asymmetry response indicating that the currents remaining after Cd do not meet this criterion for gating currents (Armstrong, 1981), i.e. $Q_{ON} = Q_{OFF}$. Similar results were obtained in 3 mM-$CdCl_2$. Note that after the Ca was replaced by Co there was a further reduction in the size

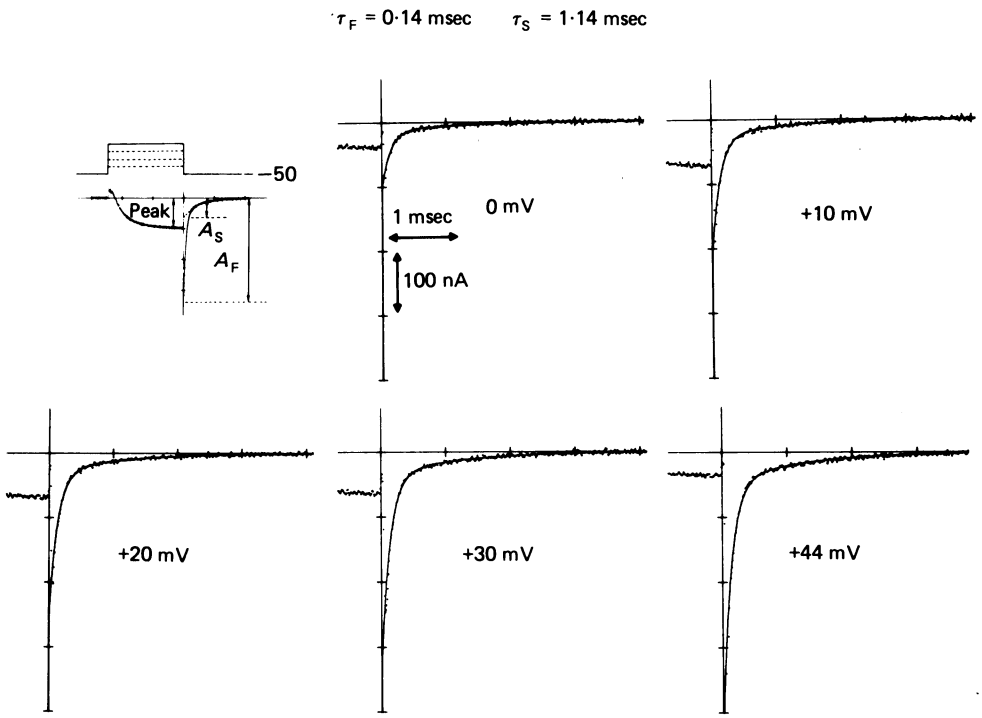

Fig. 4. Turn-off of I_{Ca}. Ca tail currents were measured at −50 mV following activation to different potentials. The parameters were estimated using the computer routine described previously and points in the first 150 μsec were not considered in the error criteria. As described in the text, from an initial approximation the time constants did not appear to be a function of the pulse potential ($\tau_F = 0{\cdot}14 \pm 0{\cdot}01$ msec and τ_S $1{\cdot}14 \pm 0{\cdot}15$ msec); the time constants were thus constrained to the mean values and the resulting curve fits are shown.

of the tail currents and Q_{ON} and Q_{OFF} were then nearly equal as was the case without the presence of Cd in the bath (Fig. 3). We interpret these results as being due to a voltage-dependent blocking action by Cd (Y. Tsuda, D. L. Wilson & A. M. Brown, in preparation).

In contrast to the result in Cd, the OFF asymmetry response in Co was sufficiently small as to have little effect on the Ca tail currents and we thus used the currents remaining after Co to make corrections where they were needed, as was done earlier (Brown *et al.* 1981). Organic Ca-channel blockers, such as verapamil and diltiazem were also examined but concentrations of tens to hundreds of micromolar were required to block completely the Ca current normally obtained (Morimoto, Tsuda & Brown, 1981) and recovery was incomplete at such high doses.

Having shown that the asymmetry component of the tail currents can be practically disregarded in our tail current measurements, we turn to an examination of the tail current components and their relationship to Ca-channel closure.

Tail current amplitude as a function of test-pulse potential and duration

The tail currents sensitive to Ca-channel blockers relax as either a sum of two or three exponentials. In Fig. 4 we show the dependence of the tail currents on pulse potential from a cell in which the tails are well described by a sum of two exponentials.

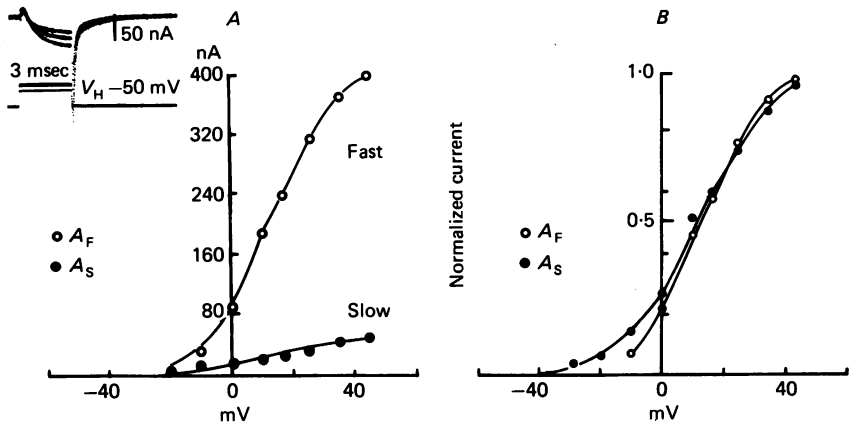

Fig. 5 *A*, amplitudes of the two tail current exponentials as functions of activating potential. A_F and A_S are the amplitudes of the fast and slow components and were obtained as indicated in Fig. 1. For reference, the maximum current obtained during a pulse was ~ 60 nA and the peak *I–V* may be seen in Figs. 4 and 5. Both A_F and A_S are normalized and are shown in *B*. Note that the 'threshold' for the appearance of the fast component is at a higher potential than that of the slow component.

Test pulses were sufficiently long for Ca currents to reach their peaks (3–4 msec), but sufficiently short to be free of any inactivation (Brown *et al.* 1981). The tails were examined following return to the holding potential of −50 mV. All of the tail currents were fitted with a sum of two exponentials for an initial estimation of the parameters. The measured time constants were well separated (fast component, $\tau_F = 0{\cdot}14 \pm 0{\cdot}01$ msec and slow component, $\tau_S = 1{\cdot}14 \pm 0{\cdot}15$ msec) and had a ratio of approximately 8 instead of the value of 2 required by an m^2 model. The distribution of the time constants showed no correlation with the pulse potential, and we concluded that the τ values were independent of the activating potential. We thus averaged the τ values for a given experiment and fitted the data again, this time constraining the values of τ to the average values; the results are shown in Fig. 4. This procedure resulted in less scatter in the plots of amplitude *vs.* pulse potential and increased our confidence in these parameter estimates; the results are shown in Fig. 5. The amplitudes of the two components, A_F and A_S, showed the normal sigmoidal voltage dependence, and A_F was considerably larger than A_S. As seen in the normalized curves in Fig. 5*B*, the curve of the A_F component is steeper than that of the A_S curve and its 'threshold' is at a more positive potential. If we assume $A_F + A_S$

to reflect the number of open channels at the end of the pulse, then a large percentage of the channels were closed at +20 mV, the potential for maximum current during the pulse, and the number of open channels did not saturate until about +50 mV or more.

We wished to test if both of these tail current components were due to Ca-channel closure. We thus tested the effect of increasing the external Ca concentration, $[Ca]_o$, on the tail currents and the results are shown in Fig. 6.

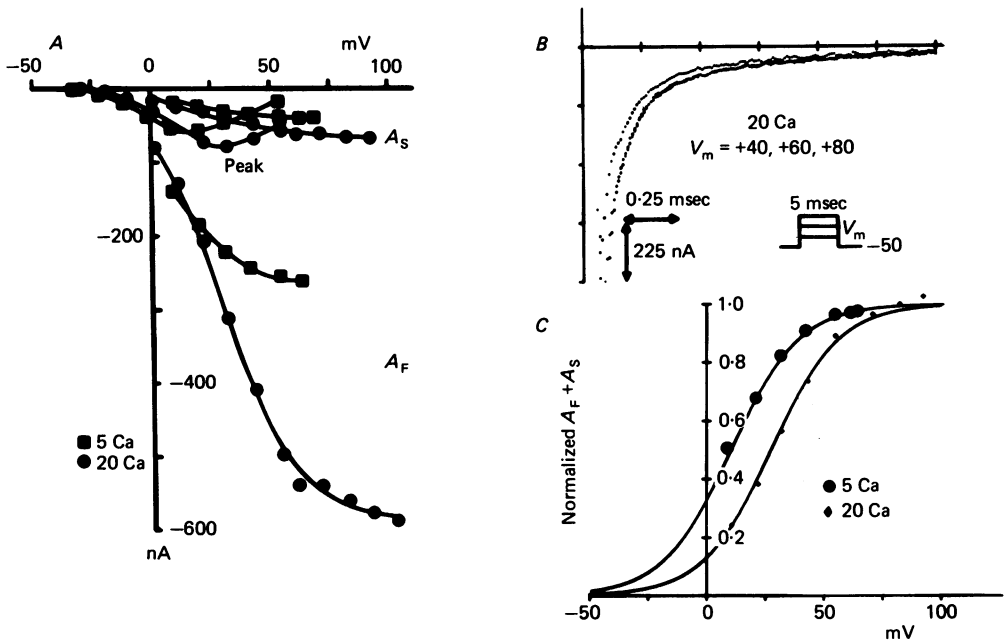

Fig. 6. Effects of increasing extracellular Ca concentration, $[Ca]_o$, on tail current amplitudes obtained at $V_H = -50$ mV and peak currents measured during the activating step. Parameter estimates were obtained as in Fig. 4 (in 5 mM-Ca, $\tau_F = 0{\cdot}16$ msec and $\tau_S = 1{\cdot}58$ msec; in 20 mM-Ca, $\tau_F = 0{\cdot}13$ msec and $\tau_S = 1{\cdot}24$ msec). *A*, increasing $[Ca]_o$ increased and shifted along the voltage axis the peak current and the amplitudes of both tail current components. Note that the A_S curve is smaller than the peak currents and that A_S is very much smaller than the A_F values. *B*, original traces which show that there was saturation of the tail currents as the pulse potential was increased. *C*, normalizing $A_F + A_S$, we obtain an activation function for I_{Ca}. Increasing $[Ca]_o$ from 5 to 20 mM results in a shift of the curve by approximately 17 mV. The smooth curves were drawn using the function $\{1 + \exp[(V - V')/F]\}^{-1}$ where $F = 14{\cdot}5$ mV, and V' is 0·5 and 27·5 mV in 5 and 20 mM-external Ca, respectively.

In Fig. 6*A* the values for A_F and A_S are clearly increased at higher $[Ca]_o$, indicating that these components are due to Ca ion flow. However, the amplitude of the fast component of the tail, A_F, was more sensitive to raising the external Ca than was A_S. Part of this was due to the fact that these currents were not corrected for the asymmetry current, and this correction of approximately 10–15 nA at positive potentials had more effect on A_S than A_F. The basis for the remaining difference in sensitivity will be discussed subsequently.

As $[Ca]_o$ was increased, there were equivalent shifts to more positive potentials of the peak I–V relationship and of the activation–potential relationship obtained by normalizing the $A_F + A_S$ values (Fig. 6*C*). This is to be expected from surface charge effects (Wilson, Morimoto, Tsuda & Brown, 1983). Interestingly, the maximum initial amplitude of the tail current, given by $A_F + A_S$, increased by a factor of approximately 2 when the extracellular concentration was changed from 5 to 20 mM whereas the maximum inward current during the pulse changed by only a factor of $\sim 1{\cdot}4$. Assuming negligible outward Ca flux at these potentials, at least two types of explanations are possible: first, a concentration-dependent change in the voltage dependence of the conductance of open channels, such as might occur from a voltage-dependent block that is relieved at the return potential; secondly, contamination from a current that is not observed at the return potential. The fact that the activation curves seem to be the same shape indicates only a simple voltage shift of the number of open channels.

The currents measured with what we call an envelope protocol are shown in Fig. 7. In this protocol, the voltage was stepped to a potential, for example +10 mV, for varying durations before returning to V_H. In Fig. 7*A*, obtained from a cell without the third component, note that the time course of the tail relaxation appears not to have changed; only the amplitude of the tail currents has changed. This observation is confirmed in Fig. 7*B* where we have fitted with constant τ values the tail currents obtained at pulse lengths of 10, 40 and 400 msec. In Fig. 7*C* we have compared the decay of the tail current amplitudes with the decay of the current during the pulse. Note that the time course of inactivation, as measured from the envelope of the tail currents, is similar to the time course of inactivation as measured from the current during the pulse. This implies that, at least in this cell, the apparent inactivation observed at +10 mV is due to a true decrease in the Ca current and is not due to contaminating outward currents. It would be quite unlikely for a contaminating current to develop without a corresponding change in the time course of the tail current relaxations. Additionally, note in Fig. 7*D* that A_F and A_S decreased equivalently as the pulse was lengthened. These results are consistent with a Hodgkin–Huxley type of formulation in which gating is the product of an activation variable and a much slower inactivation variable.

Tail currents that contain the third and slowest component

In Fig. 8 we show results from an envelope protocol on a cell which was classified as having a third component in the tail current relaxation. Note the marked increase in the time it takes for the tail to relax as the pulse duration is increased. As shown in the Figure, with the shorter pulses we were able to fit the relaxations with the sum of two exponentials, but with the longer pulses a third exponential was required to fit the relaxation. We refer to the very slow time constant as τ_{VS}, and its associated amplitudes as A_{VS}. The two time constants used to fit the data for very short pulses were also used to fit the data for the longer pulses. These results indicate a kinetic distinction between the two faster components of the relaxation and the slower component, and we have interpreted the results as being due to a Ca current which turns on rapidly (within 3 msec) and another current, as discussed later, which takes approximately 10 msec to develop fully. Interestingly, in contrast to τ_F and τ_S, τ_{VS}

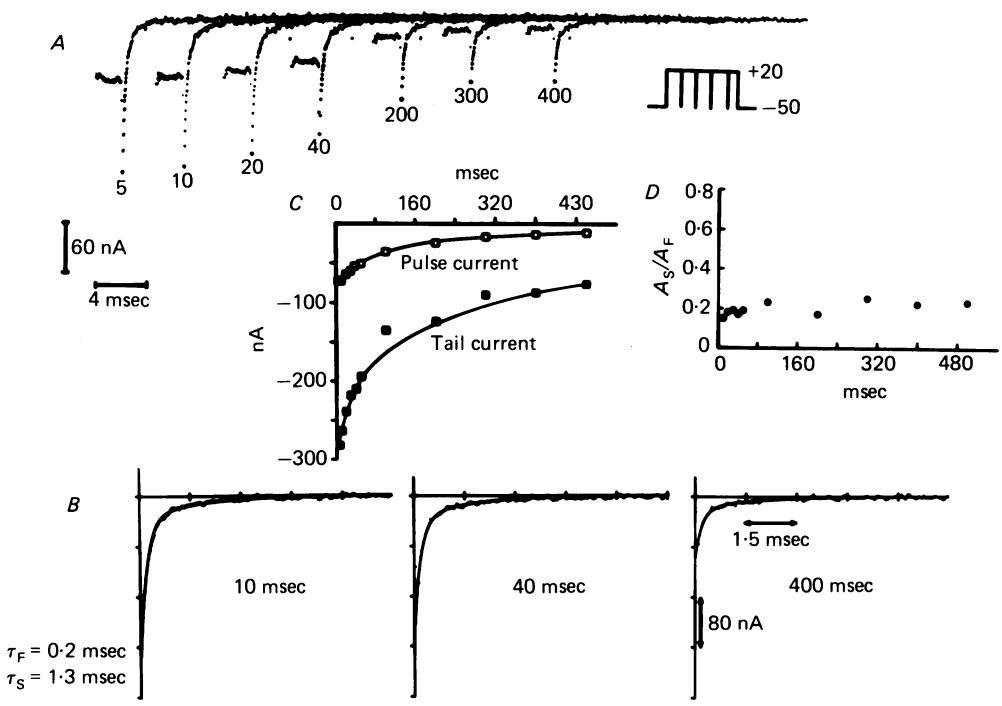

Fig. 7. The relationship of the envelope of the tails to the current during the pulse. Tail currents were measured using an envelope pulse protocol on a cell which did not have the slowest component in the tail relaxation.

A, tail currents measured after the pulse lengths indicated; the spatial arrangement has no relation to the length of the pulse. Data were digitized at 30 μsec/point, and the base line was obtained from separate current measurements.

B, there was no change in the relaxation time course of the tail currents, and fits are shown at three pulse lengths with the same τ_F and τ_S values as indicated.

C, because the tail currents following long pulses were small, we found it necessary to correct for the asymmetry current. After replacing Ca with Co, the asymmetry current obtained did not appear to be a function of the pulse duration. Several of these currents were averaged and the currents were well approximated with a single exponential having an amplitude and time constant of −15·8 nA and 0·52 msec, respectively. We thus subtracted this function from each of the currents shown in *A*. This procedure was preferable to subtracting current traces because it resulted in less noise in the signal. The resulting currents were fitted with two exponentials, the time constants were averaged, and the currents were fitted once again, this time with the τs constrained to the average (τ_F = 0·18 msec, τ_S = 1·6 msec). The amplitude, $A_F + A_S$, is the instantaneous value of the tail current, and it is plotted along with the current at the end of each pulse, designated the pulse current. Note the similarity in the decay of the two currents. After normalization, the time course of the tail envelope almost exactly reflected the decay of the pulse current during the first 200 msec (not shown).

D, the ratio of A_S/A_F as obtained in *C* is plotted as a function of the pulse duration. Note that there was little change in the ratio, indicating that inactivation is accompanied by a simple, equivalent scaling of both components of the tail relaxation.

may depend on pulse length. In another cell (not shown), τ_{VS} varied from 7 to 20 msec as the pulse length increased from 5 to 500 msec.

In Fig. 9 we show results from envelope protocols in which either Ca or Ba was used in the external solution. It has been shown that peak Ba currents at potentials up to 0 mV are larger than peak Ca currents at extracellular concentrations of 10 mM

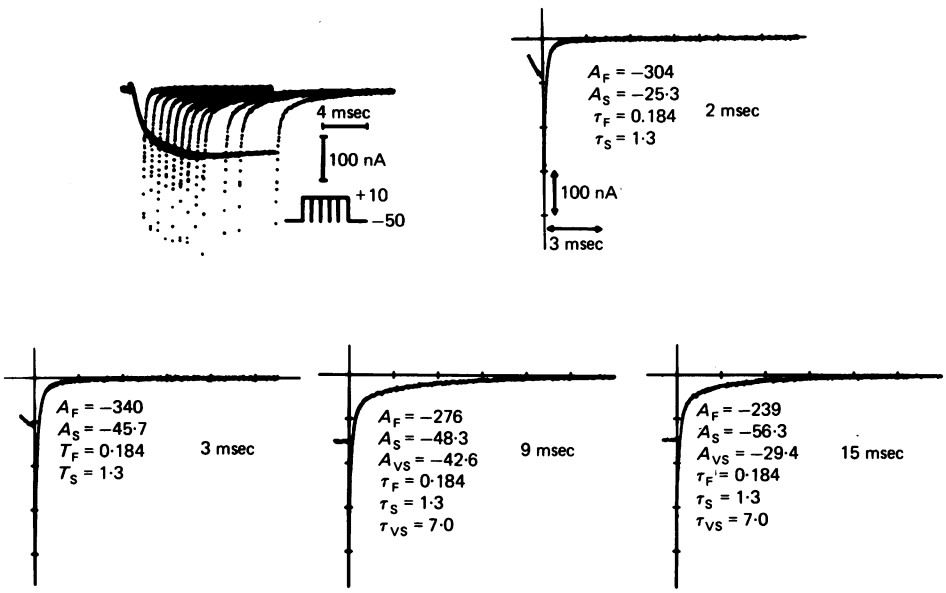

Fig. 8. Tail currents with three exponentials. Tail currents were obtained as a function of pulse length using an envelope pulse protocol as shown. Note the development of a slow third component in the tail current relaxation as the pulse is lengthened. Also shown are curve fits of the tail current at 2, 3, 9 and 15 msec pulse duration. Initially, the relaxation was fitted with a sum of two exponentials, giving τ_F and τ_S values as shown, but as the pulse was lengthened a third exponential, giving τ_{VS}, was required. Both the data points and the fitted curve are plotted. Parameters printed in the Figure are in units of nA and msec.

(Brown *et al.* 1981; Wilson *et al.* 1983). We thus wished to determine the selectivity of the tail current components to these ions. The appearance of the slowest component occurs earlier and appears much more prominent in Ba than Ca in Fig. 9*B*. In Fig. 9*A*, superimposed Ca and Ba currents obtained with 5 and 8 msec pulses are shown. In these cases, the Ba tail current is clearly much larger than the Ca tail current for several milliseconds following return to the holding potential. This result is primarily due to the difference in the way the slow component activates in Ba and Ca solutions as will be illustrated further later. In Fig. 9*C*, tail currents are shown following 12 msec pulses to +20 mV. In this case, the slow component is almost maximally activated in both ionic solutions. Note that for the first 2 msec there is a large difference in the size of the tail currents, whereas later in the relaxation, where the very slow component dominates, the two tail currents overlap closely. We interpret this result as indicating that the first 2 msec of the tail relaxation is due to a Ca-channel closure and that following this relaxation the primary source of current has changed

to a contaminating current that is relatively unspecific for Ca or Ba; similar results were obtained in another experiment in which $[Ca]_o$ was increased from 5 to 10 mM.

As is the case for the two faster components, the slowest component depends on the pulse potential. The time course of the slowest component was not always well described by an exponential with a constant τ value (the τ value may depend on pulse

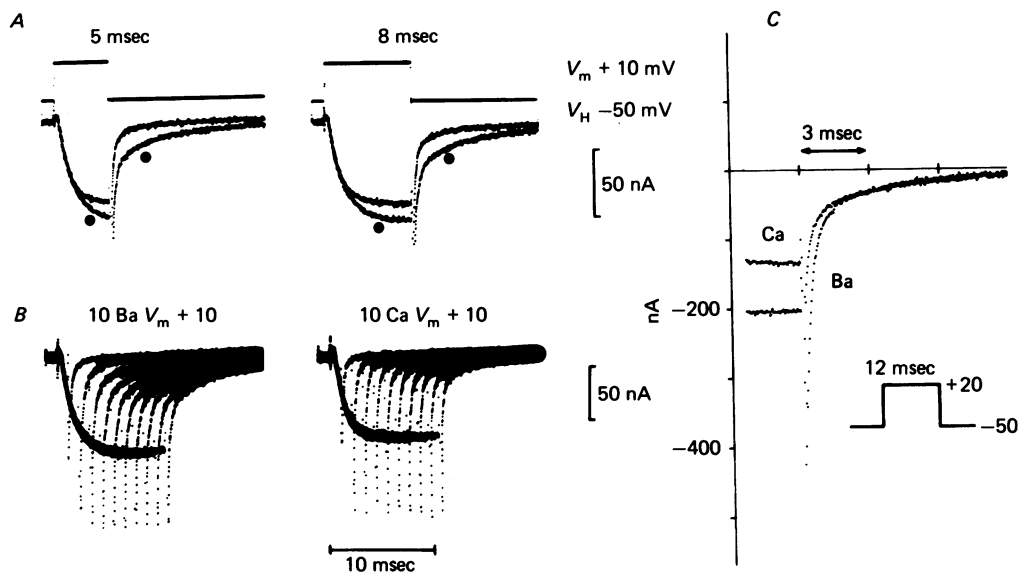

Fig. 9. Comparison of tail currents with three exponentials in the presence of Ca or Ba extracellularly, using an envelope protocol. In *B*, note that the slowest component appears earlier when Ba instead of Ca is in the external solution. In *A* traces obtained in external Ba and Ca are overlaid; currents in Ba are identified with the large filled circles. Note that with pulses of 5 and 8 msec in duration there is a significant difference in the sizes of the tail currents that lasts for several msec. In *C* are shown tail currents immediately before and after Ba substitution for Ca. In this case, a 12 msec pulse to +20 mV was sufficient to activate the slowest tail current component fully and there is a sizeable difference in the currents for only the first 2 msec. Following this the currents overlap almost exactly.

height or duration); thus, to quantify this component we used the amplitude of $I(5)$, the current obtained at 5 msec after the return of the potential to V_H, following 10 msec pulses. In Fig. 10*A* we show for Ba and Ca that A_{VS} quantified in this manner is activated by potential increases; it does not show the 'U' shape characteristic of a Ca-activated current (Meech, 1974).

In Fig. 10*B* and *C* we show the time course of the activation of A_{VS} as measured by the magnitude of $I(5)$. It takes approximately 10 msec to fully activate A_{VS}; activation is slower at −20 mV than +10 mV (Fig. 10*C*); and activation is slower for Ca than Ba. Note that although the first two components of the tail current relaxation are always present and are fully activated at 3–4 msec, the activation of the A_{VS} component requires more time to develop. The results of Fig. 10*A* indicate

that there may be a voltage shift of the activation curve for A_{VS} when Ca is replaced by Ba externally. This would be consistent with external Ba and Ca effects on surface charge (Wilson *et al.* 1983). Note also that the amplitudes of $I(5)$ obtained in this Figure for $[Ba]_o$ and $[Ca]_o$ are approximately the same after taking into account this shifting effect.

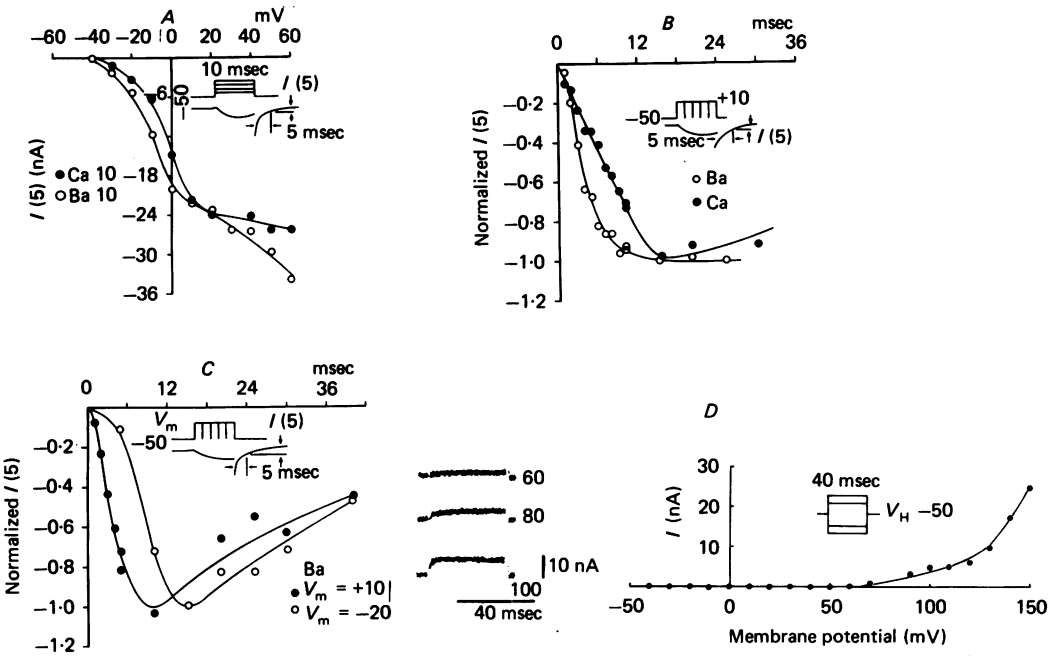

Fig. 10. Activation of A_{VS} in Ba and Ca tail currents and a comparison of A_{VS} with I_{NS}. *A*, A_{VS} activation in Ba and Ca tail currents as a function of pulse potential. Plotted is $I(5)$, the size of the current at 5 msec following the return of the potential to V_H. Note that the difference in the size of the currents obtained in Ca and Ba is approximately accounted for by a 10 mV shift of the Ca curve along the voltage axis. *B*, time course of A_{VS} activation for Ca and Ba currents as measured with $I(5)$. Note that the development of A_{VS} is slower in Ca than Ba. *C*, time course of A_{VS} activation at two different potentials as measured with $I(5)$. Note that the time-to-peak decreases as the pulse potential amplitude increases. Also note that $I(5)$ decreases as the pulse duration increases and that this effect is more marked in *C* than in *B*. *D*, time course and voltage dependence of I_{NS} as measured in another cell. I_{NS} is the current obtained after Co replacement for Ca and subtraction of linear leakage currents by summation of equal and opposite polarity voltage pulses. Asymmetry currents were not resolved in this experiment. Note that there is no significant tail current left even when the cell has been depolarized to +100 mV. The *I–V* curve for I_{NS} plotted in *D* is different in shape and is displaced to much more positive potentials than the activation curves for A_{VS} plotted in this Figure.

Byerly & Hagiwara (1982) have indicated that A_{VS} may be related to the non-specific outward current (I_{NS}) obtained after Ca current block (Brown *et al.* 1981). In Fig. 10*D*, we show the I_{NS} current which in robust cells fully activates in ~ 3 msec (Brown *et al.* 1981). Thus, I_{NS} and A_{VS} are kinetically distinct. Also note that there are no large slow tail currents obtained at V_H after Co replacement (Figs. 3 and 10*D*), and

the activation curve for I_{NS}, as compared to that of A_{VS}, is very much different in shape and is displaced to much more positive potentials. We designed additional experiments to establish the reversal potential of the current which gave rise to the slowest component of the tail current relaxation. However, at return potentials increasingly more positive than -50 mV the slowest tail current component became vanishingly small and difficult to distinguish from the relaxation components resulting from inactivation and recovery from inactivation.

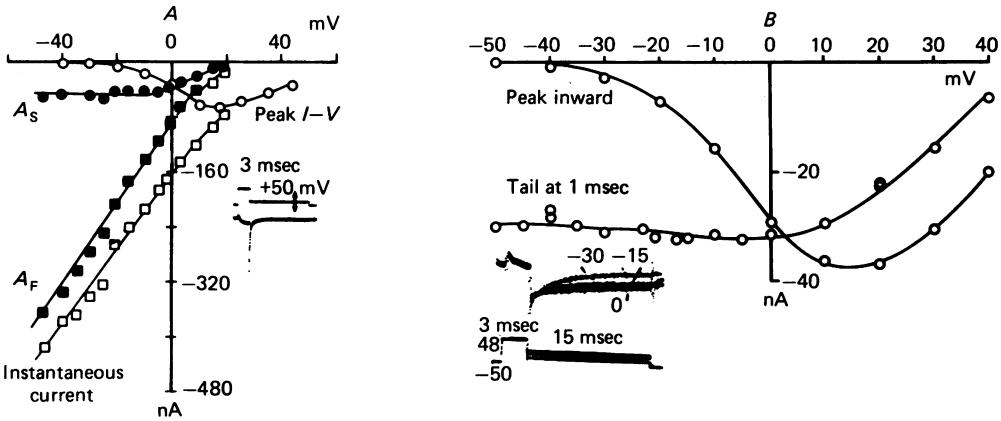

Fig. 11. Instantaneous I–V relationship determined from tail current amplitudes according to the protocol shown in the bottom inset of A and the inset of B. A, tail currents were fitted with the sum of two exponentials, with amplitudes A_F and A_S, and a constant value determined by the value of the current at the end of 5 msec. The instantaneous current is the sum of these three terms. A_S (●) is independent of potential between -50 and 0 mV but A_F (■) and the instantaneous current (□) are linear functions of potential over this range. The peak I–V curve is also shown, and it was obtained according to the protocol shown in the top inset of A. B, from another cell, the value of the tail current at 1 msec is plotted along with the peak current during the pulse. Note that this gives a curve which is significantly distorted from the instantaneous I–V as expected from the results in A.

Instantaneous I–V relation

In these experiments, the potential was stepped to +46 mV for 3 msec to obtain maximal activation and then returned to different potentials (Fig. 11). Linear components of leakage current and capacitive transient were cancelled by adding a hyperpolarizing pulse which was the mirror image of the depolarizing pulse shown in the inset. We fitted the resulting relaxations with the sum of two exponentials and a constant, and thus obtained A_F, τ_F, A_S, τ_S, and the steady-state amplitude, A_{SS}, as functions of potential.

In Fig. 11A we have plotted, as functions of recovery potential, the amplitudes of A_F, A_S, and $A_F+A_S+A_{SS}$, the latter sum giving the instantaneous I–V curve for the Ca current. Note that A_S is constant from -50 mV to +10 mV, whereas A_F shows a linear dependence on voltage. The instantaneous current, A_F+A_S, is dominated by the A_F component over most of the voltage range studied, and it becomes

increasingly negative as the potential is hyperpolarized. This instantaneous I–V curve is very different from measurements published earlier (Kostyuk *et al.* 1981; Llinas *et al.* 1981) but seems to agree with the observations of Fenwick *et al.* (1982) and Byerly & Hagiwara (1982). It appears possible that the reason for the differences may be that the faster component was not resolved in the earlier reports as shown in Fig. 11*B*. There the plot of the tail current at 1·0 msec *vs.* potential is flat at negative potentials.

We may now re-examine the results in Fig. 6, where we found that A_F was more sensitive than A_S to changes in $[Ca]_o$. In Fig. 11*A* between −50 and 0 mV, A_F changes much more than A_S as a function of the recovery potential. We assume the removal of channels from the open state, and thus the relative size of A_F and A_S, to be governed by the values of the rate constants at the recovery potential. We also may expect that surface charge effects may shift the voltage dependence of such rate constants in a manner similar to that measured from the turn-on process as revealed in the peak I–V curves (Wilson *et al.* 1983). Thus, in the case of high extracellular Ca, we might expect the curves in Fig. 11*A* to be shifted along the voltage axis to more positive potentials. At a given potential, in this case −50 mV, we might expect A_F to increase more than A_S in going from 5 mM- to 20 mM-Ca.

From an instantaneous I–V curve and an activation curve, both of which were obtained from tail current measurements following 3 msec pulses, we have constructed an isochronal I–V curve and have compared it to an isochronal I–V obtained from measurements during voltage-clamp pulses. These curves are very close to the peak I–V curve since activation is normally complete at 3 msec. We assume the following simple model for the peak current

$$I_P(V) = O(V) \times NF(V), \tag{1}$$

where N is the number of channels, $F(V)$ is the single channel current as a function of voltage, and $O(V)$ is an activation function which in the case of a single open-state channel is the probability of the channels being open. We assume $O(V)$ to be given by the normalized instantaneous value of the tail currents obtained as a function of the pulse potential, as shown in Figs. 5*A* and 12*A*. The $NF(V)$ is the instantaneous I–V obtained from plotting the initial values of the tail current *vs.* the recovery potential.

The instantaneous I–V relation must asymptotically approach the zero current axis at depolarized potentials because the peak I–V of the Ca current is never outward over the voltage range studied (Brown *et al.* 1981). Additionally, such an asymptotic form is obtained from the constant-field equation because the outward going flux is negligible in the case of the highly asymmetric Ca concentrations present ($[Ca]_i = 10^{-8}$ and $[Ca]_o = 10$ mM). We found the instantaneous I–V relation to be somewhat less steep in form than that given by the constant-field equation, and it was best fitted (Fig. 12*B*) by the modified form shown below, where V is the applied voltage and P, H, and V' are constants. The parameters for the fit are indicated in the Figure legend.

$$NF(V) = P \times (V - V') \frac{[Ca]_o \exp(-2V'/H)}{1 - \exp[2(V - V')/H)]}. \tag{2}$$

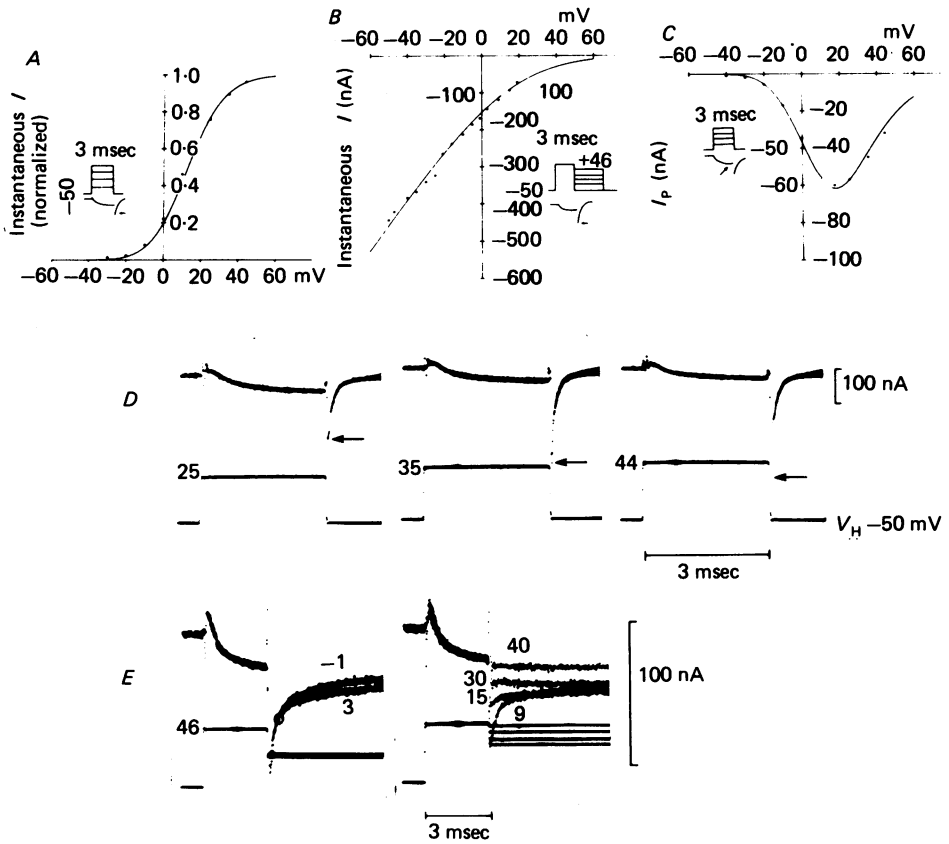

Fig. 12. Construction of the peak I–V curve and a paradox in the instantaneous I–V. A, the activation curve is obtained by normalizing $A_F + A_S$ obtained in Fig. 2. The data points are fitted with eqn. (3) of the text and the parameters for the fit are $V_1' = +12{\cdot}8$ mV and $V_2' = -27{\cdot}2$ mV. B, instantaneous I–V relationship obtained from Fig. 4. The data points are fitted with eqn. (2) of the text and $V' = 15$ mV, H = 25·8 mV, and $P = 2{\cdot}241 \times 10^3$ nA/mV . mM. C, constructed peak I–V relationship (continuous curve) and the peak I–V (●). The constructed I–V was obtained by multiplying the function describing the activation curve in A and the function describing the instantaneous I–V in B. Parameters were the same as in A and B with the exception that P was increased by a factor of 1·23 from $2{\cdot}241 \times 10^3$ nA to $2{\cdot}764 \times 10^3$ nA. This value may be expected since between the two runs there was a decrease in the control current by a factor of 1/1·18. D and E, raw current traces which show paradoxical flatness in the tail current relaxation. From the original traces in D we can see that activation does not saturate below +40 mV; i.e. the tail current, indicated by the arrows, is increasingly inward as the pulse potential increases from left to right. In E we show tail currents obtained at various return potentials as indicated by the numbers on the Figure. Note in E (right) that upon returning the potential to +30 mV, the tail current appears to be flat. This occurs despite the fact that in stepping the voltage from +46 to +30 mV, the change along the activation curve in A is 14 %.

We also fitted the activation curve as shown in Fig. 12*A* with an equation of the form

$$O(V) = \{[1+\exp(V_2'-V)]^2 \exp(V_1'-V)]+1{\cdot}0\}^{-1}, \quad (3)$$

where the parameters are once again indicated in the legend. The form of this latter equation is not unexpected. It may be obtained from the steady-state solution of the four-state model suggested later using Boltzman distributions for the function of the rate constants *vs.* potential. We obtained the peak *I–V* curve in Fig. 12*C* by multiplying the function representing the activation curve and the instantaneous *I–V* curve. Note that the fit of all three curves to the data points is quite good and recall that the constructed *I–V* was obtained from tail current measurements alone.

We found an apparent paradox in the instantaneous *I–V* experiments. In Fig. 12*A* we see the activation curve does not saturate until approximately +50 mV and that in going from +30 to +46 mV there is a 14% change in the activation curve. This is confirmed by the original traces present in Figs. 12*D* and 6*B*. Thus, one would expect a significant relaxation in the tail current when the return potential is +30 mV. Note that in Fig. 12*E* the tail current is almost flat at +30 mV but is net inward. We believe that at this potential there is no significant slow component present in the relaxation in a voltage step between these two potentials, and the fast component of the relaxation has become too small and too fast to resolve. Some indication of this is shown later when the time constants of the relaxations are presented in more detail.

Having established the relationship between the number of activated, open channels and potential, and the conduction process in these opened channels, we turn now to a consideration of the rates at which the channels open.

Turn-on of I_{Ca}

The turn-on of the Ca current is shown in Fig. 13. As discussed earlier, linear components of capacitive and leakage currents have been removed, and the asymmetry current has also been subtracted. The latter is important because the asymmetry current dominates during the earliest part of activation as reported by Kostyuk *et al.* (1979, 1981). The corrected currents clearly turn on with an initially flat portion which is usually described by a Hodgkin–Huxley variable raised to a power. However, as shown previously the two τ values obtained from the tail current relaxation have a ratio greater than 6 and this rules out an m^2 description. This discrepancy first led us to fit the corrected turn-on currents with a general three-state model in which the rate constants are assumed to be functions of potential (Fitzhugh, 1965; Armstrong, 1981; Hahin & Goldman, 1978*a*, *b*; Fenwick *et al.* 1982). One open state was allowed which is consistent with the single-channel results of Lux & Nagy (1981), Fenwick *et al.* (1982) and Brown, Camerer, Kunze & Lux (1982). The scheme of the model is

$$R \underset{k_{-1}}{\overset{k_1}{\rightleftharpoons}} A \underset{k_{-2}}{\overset{k_2}{\rightleftharpoons}} O, \quad (4)$$

where R, A, and O are the probabilities of the channels being in the resting, activated and open states respectively; the k's are the voltage-dependent rate constants; and

the conservation equation, $R+A+O=1$, is imposed. The solution for the system of equations governing this reaction scheme is

$$I = G\left(1+\frac{\tau_1}{\tau_2-\tau_1}e^{-t/\tau_1}+\frac{\tau_2}{\tau_1-\tau_2}e^{-t/\tau_2}\right), \tag{5}$$

where we have imposed the boundary conditions $O(t=0)=A(t=0)=0$ and $R(t=0)=1$ (Chiu, 1977) and where G is a function of voltage that should be equivalent to the instantaneous I–V relation (i.e. $NF(V)$). These boundary conditions

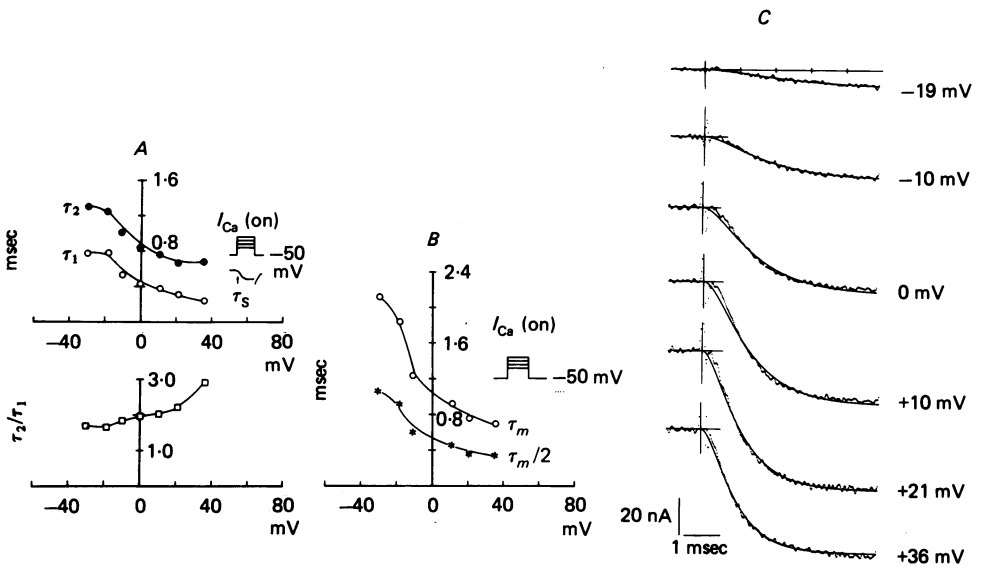

Fig. 13. Turn-on of I_{Ca}. Ca currents at different potentials are shown in C and the smooth curves are m^2 curve fits as described subsequently. The currents have been corrected for linear components of leakage and capacitance and for the initial, outward asymmetry current. The delay in the turn-on is clear. Time constants from the fits of turn-on to a general three-state model (eqn. (5)) are shown in A. Note that the ratio τ_2/τ_1 is close to 2 over most of the potential range. τ_m and $\tau_m/2$ obtained from fits to an m^2 Hodgkin–Huxley model are shown in B.

are imposed in order to obtain the zero initial derivative in the Ca current turn-on as is shown at small depolarizations in Figs. 13 and 17. The argument proceeds as follows. The differential equation describing the probability of being in the open state is $dO/dt = k_2A - k_{-2}O$. Since $O(t=0)=0$ and $dO(t=0)/dt=0$, it follows that $A(t=0)=0$. An additional rationale for these boundary conditions is presented later. The relationship between the time constants, τ_1 and τ_2, and potential is shown in Fig. 13A. The ratio of τ_2 to τ_1 is very nearly 2 over the potential range examined, which is the ratio expected for an m^2 model. This, together with the fact that Kostyuk *et al.* (1979, 1981) had reported agreement with an m^2 fit, encouraged us to use the m^2 model which is a particular version of the scheme in eqn. (4), i.e. $k_1=2\alpha$, $k_{-1}=\beta$, $k_2=\alpha$, $k_{-2}=2\beta$. The result is

$$I = G(1-e^{-t/\tau m})^2 = G(1-2e^{-t/\tau m}+e^{-2t/\tau m}). \tag{6}$$

The fit to the turn-on data and the plots for τ_m and $\tau_m/2$ *vs.* potential are shown in Fig. 13.

Having shown that turn-on is fairly well described by an m^2 process we can now compare the turn-on results with the tail or turn-off results.

Comparison of turn-on and turn-off current kinetics

The tail current τ values extracted by exponential fits to the tail currents were shown in detail in Fig. 4 and their relationship to recovery potentials is shown in Fig. 14. Only τ_F and τ_S were present in this cell. Some important points are revealed by

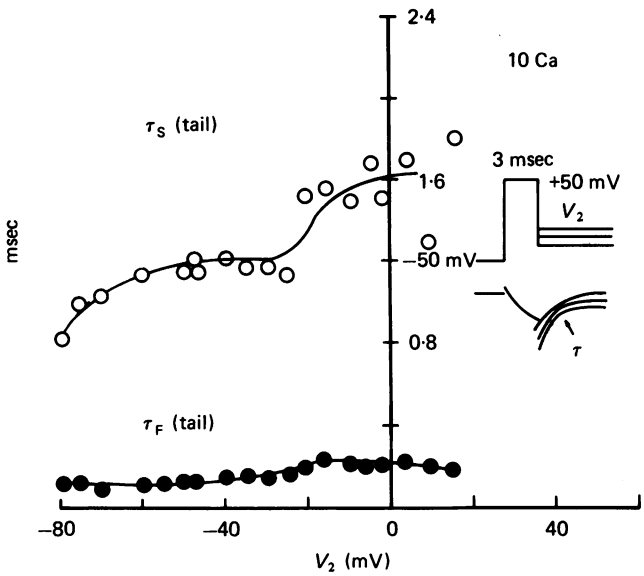

Fig. 14. Relationship between tail τ's and potential. This plot is compared with the turn-on τ values in Fig. 13 as described in the text.

a comparison of τ_F and τ_S in Fig. 14 with those of τ_m and $\tau_m/2$ which were plotted in Fig. 13*B*. First, τ_F is very much faster than $\tau_m/2$; secondly, the ratio of τ_F to τ_S is variable and is between 6 and 8 which is very much greater than 2, the ratio expected for an m^2 model; thirdly, the voltage dependence of τ_F is small and appears to be different from that of the τ_m values; fourthly τ_S has values similar to those of the τ_m. To expand on the latter point, at -40 mV τ_S is almost equal to $\tau_m/2$ and the m^2 Hodgkin–Huxley model predicts a tail current dominated by an exponential with a time constant of $\tau_m/2$. At more depolarized potentials τ_S may be viewed as resulting from a single exponential fitted to a weighted sum of exponentials with time constants of τ_m and $\tau_m/2$. The results suggest that the tail or turn-off currents contain the τ_m and $\tau_m/2$ components of the turn-on or activation currents and an additional process that is very much faster. These points will be dealt with later in terms of the constraints that they place on a minimum model of activation. The distinction between the time courses of turn-on and turn-off is further emphasized by the effects of temperature described next.

Temperature effects on turn-on and turn-off

Initially the effects of lowering the temperature to as low as 15 °C were examined; however, we found incomplete recovery at this temperature. This result seems to be specific for I_{Ca}, and we did not find it to be the case for recovery of K currents (Y. Tsuda, A. Yatani & N. Akaike, in preparation). We thus restricted the temperature to 18 °C, and above, where recovery was complete. Cooling produced a marked depression of the peak current, and a marked slowing of the turn-on of the currents

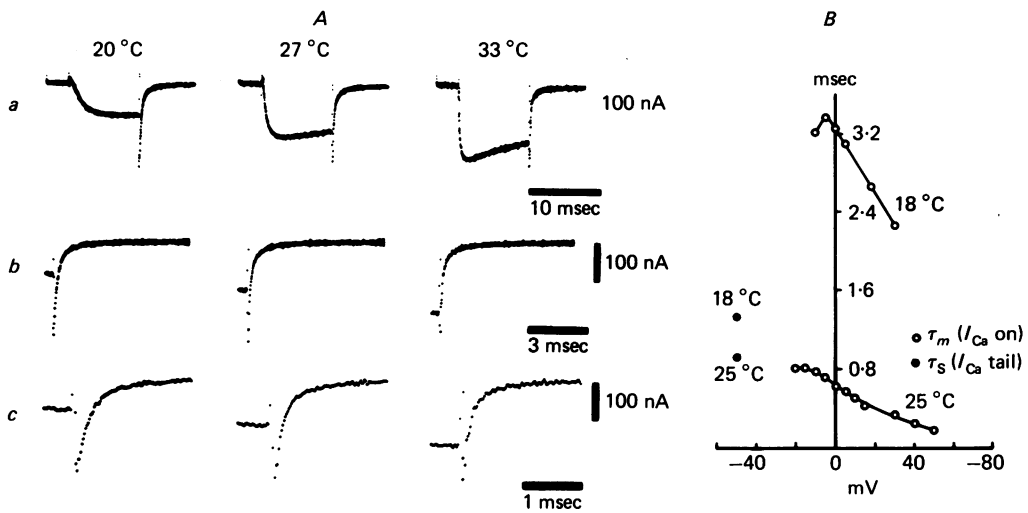

Fig. 15. *A*, effects of temperature changes on Ca currents at +25 mV in *a* and on tail currents following a step to +50 mV in *b* and *c*. V_H was −50 mV. Note the different time scales in *a*, *b* and *c*. *B*, from another cell, turn-on was fitted using eqn. (7) at two different temperatures. τ_m is plotted as a function of the pulse potential and τ_S from the tail current obtained at V_H is also plotted.

(Fig. 15*A*). In addition inactivation was much slowed by cooling, and in Fig. 15*A* there is no apparent inactivation at the coolest temperature. In contrast to the turn-on response, there was very little effect on the rates of relaxation of the tail currents at V_H as shown in Fig. 15*A*.

In many experiments we did not make measurements of the asymmetry ON current at different temperatures so that accurate correction for the asymmetry current was not possible. In order to estimate the rate of turn-on of these currents, we fitted the data with a model which had an m^2 term to account for the ionic current plus another term to account for the outward asymmetry current. Kostyuk *et al.* (1981) have reported that above −5 mV the asymmetry current for turn-on may be approximated by a single exponential having a time constant equal to τ_m, the same parameter obtained from fitting the ionic current with an m^2 model. At potentials more negative than −5 mV there was not a large difference in the time constants, and the contribution of the asymmetry current was small. These results have been confirmed by for the most part our own measurements (Y. Tsuda, D. L. Wilson & A. M. Brown, unpublished observations). Thus, the model chosen to fit these data was

$$I = G_1(1-e^{-t/\tau_m})^2 + G_2 e^{-t/\tau_m}, \quad (7)$$

where G_1, G_2 and τ_m were the varied parameters.

Fig. 15*B* shows that τ_m was very much slowed over the entire voltage range studied. Also shown in this Figure are the τ_S values measured from the tail current obtained at V_H. The Q_{10} for τ_m was greater than 6·5, whereas the Q_{10} for τ_S was 1·9.

We also examined the effects of temperature on the A_{VS} component of the tail current (Fig. 16). Note that although there is a large effect of temperature on the

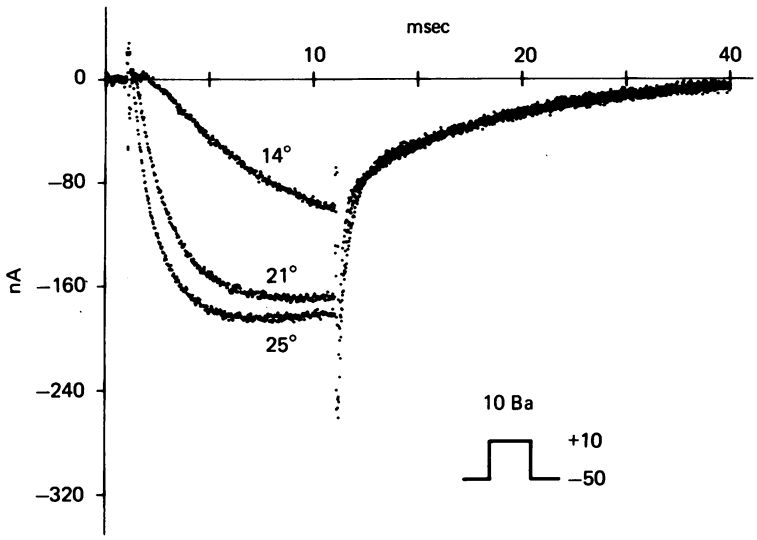

Fig. 16. Effect of temperature on tail currents. Cooling slows turn-on and reduces the amplitude of the current during the pulse. The amplitudes of the early components in the tail, A_F and A_S, are reduced by cooling, but neither the amplitude nor the time course of the A_{VS} components is affected by cooling.

amplitude of the peak current and the kinetics of turn-on, there is very little effect on the amplitude or the kinetics of the relaxation of the tail after 1–2 msec has passed. Early in the relaxation of the tail there is a decrease in the amplitude of the tail currents with cooling, and this we interpret as amplitude changes of A_F and A_S. This experiment again indicates that the two faster components are due to a different process than that of A_{VS}. Both the kinetics and amplitude of A_{VS} are peculiarly insensitive to temperature effects.

We are faced with what seems to be a paradox. The turn-on response of the Ca current is fitted quite well with an m^2 model, but the turn-off response is not; the turn-on response is very temperature-sensitive, the turn-off response is not. In the next section we attempt to reconcile these differences.

A model for activation

If we restrict ourselves to transition-state models with voltage-dependent rate constants such as are currently in vogue for describing the time course of ionic currents, then we are immediately led to certain restrictions on a model for activation that follow from linear systems theory (Swisher, 1976; Colquhoun & Hawkes, 1977). First, the step response at a given potential will be a weighted sum of exponentials,

the time constants of which will be determined by the rate constants at that potential. The time constants in the system response do not depend on the past history of the potential; the relative weight, or amplitude, associated with each exponential will, however, depend on the past voltage history. Secondly, the order of the system of independent differential equations describing the state-transition diagram is equal to the number of states minus one; it follows that the number of exponentials in the system response is also one less than the number of states in the system. Let us consider these points in reviewing the salient points from the data in Figs. 13 and 14. First, focus on the potential range where the data overlap, that is from -50 to -20 mV. The τ_S measurements are comparable to the τ values obtained from the turn-on response, i.e. τ_m and $\tau_m/2$, but there are no values that compare with τ_F in the turn-on response data. These observations indicate that at a given potential below 0 mV at least three distinct exponentials are measurable from the I_{Ca} response to pulse protocols designed to study the activation process. The three exponentials are indicated by τ_F, τ_m and $\tau_m/2$. In our view, the τ_S measurement is indicative of a measurement which is a weighted sum of two exponentials with time constants τ_m and $\tau_m/2$. These three modes in the system response indicate that there must be at least four states in the state-transition diagram.

In Fig. 17*B* we show several current traces which clearly indicate that a three-state model is not applicable. These were obtained from different cells with potential steps near threshold. The traces were fitted with the three-state model (eqn. (5)), and the time constants from the fits are shown in the Figure. Note that the initial flat portion of the turn-on is very long, indicating that two slow time constants are required in eqn. (5) to describe the response. As expected, both time constants from the curve fits are much greater than the values of τ_F. For turn-on at potentials more positive than 0 mV, it is possible to obtain a reasonable fit to the delay in the turn-on using the three-state model with one of the time constants constrained to the τ_F value; such a conclusion was reached by Fenwick *et al.* (1982). However, in the critical region near threshold a three-state model is clearly not applicable.

Temperature effects provide additional evidence that is not easily reconcilable with a three-state model. In Figs. 15 and 16, note that the time course of the tail currents at -50 mV are practically unchanged by a change in temperature, whereas the time course of the turn-on response is markedly affected in the potential range between -20 and $+50$ mV, as seen in Fig. 15*B*. In Fig. 17*C* we show the effects of temperature on original current traces obtained with depolarizations near threshold. Note that the decrease in temperature markedly increases the length of the initially flat portion of the turn-on response; the current is practically zero for 1·5 msec, and slow time constants are obtained from the fit. This occurs despite the fact that at -50 mV there is little change in the time course of the measured tail currents. These effects extend to the range between -20 and -50 mV (H. D. Lux & A. M. Brown, in preparation), and the present result indicates that turn-on must involve an exponential very different from the two uncovered by the turn-off response at -50 mV. This result is difficult to reconcile with a three-state model since only two modes are present in the system response. Such responses are possible, however, with a sequential four-state model in which the leading forward rate constant is zero at -50 mV and is markedly temperature dependent, as shown later.

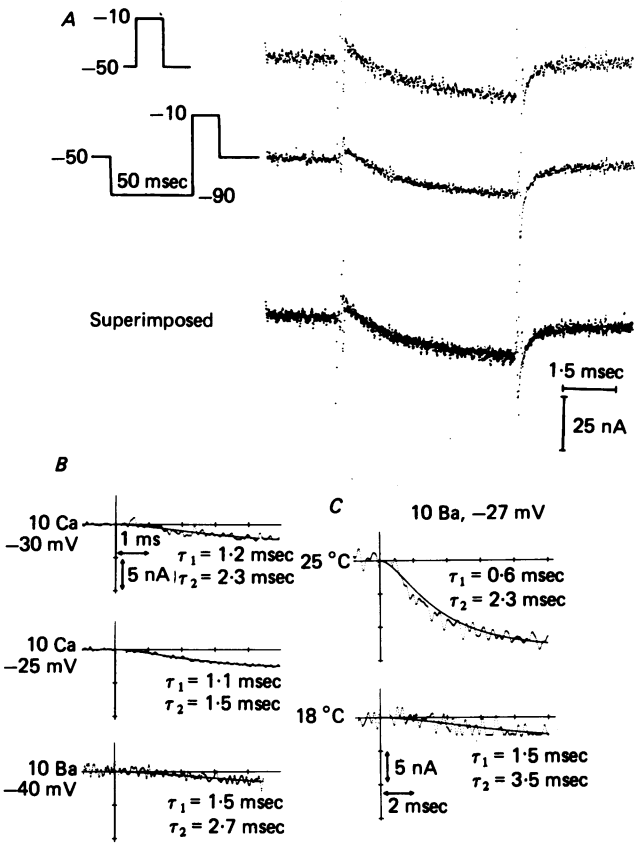

Fig. 17. Selected traces which establish certain restrictions on a model describing Ca current activation.

A, changing the holding potential from −50 to −90 mV resulted in no change in the amplitude or time course of the current resulting from a depolarizing pulse. This indicates that there was no change in the initial conditions for the system as a result of the change in V_H.

B, turn-on near threshold for I_{Ba} and I_{Ca} from three different cells. The low signal-to-noise ratio results from the very small currents being measured. (Average of either 10 or 50 traces.) The top trace was from the same cell in Fig. 6. The middle trace is from another cell in which the currents were averaged fifty times. In 10 mM-Ba (bottom trace), threshold is at a more negative potential than for Ca, and we may obtain turn-on values at more negative potentials. The crucial point to note in all of these measurements is the duration required for the currents to become non-negligible. Because of the poor S/N, convergence of the fits to eqn. (5) was not as good as in other measurements. Various initial conditions were tried and the curve fits shown were those with the smallest sum of the squared error values obtained. The τ values shown indicate clearly that a three-state model is inappropriate in this potential range because the τ values are much different than those obtained from turn-off at the same potentials.

C, effect of cooling on turn-on near threshold. Cooling resulted in an increase in the τ values for the fit of eqn. (5) to turn-on, whereas the turn-off response at −50 mV was unaffected (Fig. 8). (Average of five traces.)

In Fig. 17*A* we also show that the response to a depolarization to −10 mV is unchanged when the holding potential is hyperpolarized from −50 to −90 mV. This indicates that the initial conditions for turn-on are the same in either case. The simplest explanation is that in both cases the initial conditions for a state-transition model such as that in (4) are $O(t = 0) = A(t = 0)$ and $R(t = 0) = 1$ as described previously. In order for these initial conditions to hold in the three-state model, the leading forward rate constant, k_1, must be zero at −50 mV. An m^2 model can be excluded on these grounds also because it would permit only one time constant in the tail current at this potential.

Since we had ample evidence that a three-state model was insufficient to describe our results, we have begun to investigate four-state models with simple structures such as the one shown below where A_1 and A_2 are activated states, R is the resting state, and O is the open state.

$$R \underset{\beta}{\overset{2\alpha}{\rightleftharpoons}} A_1 \underset{2\beta}{\overset{\alpha}{\rightleftharpoons}} A_2 \underset{b}{\overset{f}{\rightleftharpoons}} O. \tag{8}$$

We have imposed the restrictions on the rate constants for the first two transitions to attempt to mimic the m^2 behaviour of turn-on. Unfortunately, even with this simple structure an analytical solution of the resulting system of equations is quite difficult, and for the most part is so complex as to make it unwieldy. We will report here some preliminary results from numerical simulations which we feel may help to explain some of the Ca current characteristics. With the model shown, we have found that it may be quite reasonable for the fast component to be hidden during turn-on. This occurs if the rate constants $f(V)$ and $b(V)$ are relatively large, which requires that the transitions between A_2 and O are very much faster than the other transitions. Thus, during turn-on the rate-limiting steps in the transition from R to O occur in the first two transition steps, and the dynamics of the last transition may remain essentially hidden. During turn-off there may be, depending upon the voltage dependence of the rate constants, an initial rapid decrease in the channels from the O state to the A_2 state followed by a slowing of the relaxation as the A_2 state fills up. The simulations thus indicate that with the proper choice of rate constants it may be possible to have a turn-on response in which the time course yields information about only two of the three modes of the system. Turn-off is simply better suited to elicit the third fastest mode. This occurs despite the fact that from a theoretical point of view the system is completely observable and each of the modes should be seen in the system response (Swisher, 1976). The effects of cooling may be explained by the following argument. First, preliminary simulations indicate that the rate of turn-off is relatively insensitive to the leading forward rate constant. Secondly, if this rate constant turns out to be relatively small, then it may be more sensitive to changes in temperature than the other rate constants (Adamson, 1973). Thus, together, these effects may lead to an explanation of our result that turn-on is very much slowed by decreases in temperature whereas turn-off is not. Perhaps this is evidence for a metabolic step in the turn-on of the Ca current. These modelling results will be presented more fully later.

DISCUSSION

Validation of the method

Ca tail currents are large and fast; accurate measurement requires knowledge of the performance characteristics of the voltage clamp and preparation. We have made several important improvements in the voltage-clamp system which are described in the Methods and have established the following points.

(a) The voltage clamp completes the voltage transition in approximately 30 μsec and the large initial component of the capacitive current transient is 95 % complete in about 60–80 μsec.

(b) An evaluation of R_S from frequency domain techniques indicates that it is < 5 kΩ which is much smaller than previously reported (Brown *et al.* 1981). After the 100 μsec required for the fast capacitive transient to subside, the voltage drop across R_S is less than a millivolt.

(c) Impalement of several cells with a second micro-electrode 'outside' the clamp circuit indicated that spatial control was excellent.

We also wish to point out the theoretical advantage in using a two-pipette technique. As noted by Eisenberg & Engel (1970), a single electrode clamp may have poor spatial control because the current source arises from a finite space and this results in a spatial dependence of the voltage due to the high current density in this region. Perhaps the high spatial uniformity achieved with our technique is not possible with a single electrode clamp no matter what kind of access resistance compensation is used.

In addition to these checks on our method we have adopted a rather conservative approach and we do not measure the data collected in the first 100–150 μsec after a voltage transition. We have assumed that the current relaxations are composed of sums of exponentials, and we may thus extrapolate the model fit to time zero to give instantaneous current values.

Which tail current components are due to Ca-channel closure?

Our results may be compared with recent reports on Ca tail currents by Byerly & Hagiwara (1982) in molluscan neurones and Fenwick *et al.* (1982) in mammalian chromaffin cells. The former found three components in the tail currents, as we did, but attributed only the fastest of them to a Ca current and identified the other two components as arising from I_{NS}. Fenwick *et al.* (1982) observed two components and attributed both to Ca currents. The two faster components that we have identified have relaxation rates comparable to those observed by Fenwick *et al.* (1982) and, for reasons given in the next paragraph, we conclude also that the two faster components we observed are due to closure of Ca channels. We may reconcile our observation of a third slow component with those of Fenwick *et al.* (1982) because it is possible that the slowest contaminating component of the tail currents is absent in chromaffin cells. We may point out additionally that Fenwick *et al.* (1982) used pulses that may not have been sufficiently long to activate a significant A_{VS} component in the tail relaxation. The differences with the conclusions of Byerly & Hagiwara (1982) are not so easily resolved.

Let us consider the evidence that the current which gives rise to A_{VS} is distinct

from the current which gives rise to the other two components. Unlike Byerly & Hagiwara (1982), we find in going from external Ca to Ba a clear difference between the size of the tail currents at times when the two fastest tail current components dominate (Fig. 9). Similar results were obtained when $[Ca]_o$ was changed (not shown). Changing $[Ca]_o$ in a cell with no A_{VS} component clearly increased the size of the A_F and A_S components, as shown in Fig. 6. There is a kinetic distinction between the activation of the components of the tail current; the two fastest components are always present with very short pulses whereas the slowest component is not significant until $\gtrsim 8$ msec of the pulse has elapsed in the case of 10 mM-Ca. An even more compelling argument that A_{VS} is due to a different process is the fact that in some cells we observed the two faster components but we did not observe the A_{VS} component. As pointed out earlier, the temperature experiment (Fig. 16) also supports the idea that A_{VS} is due to a different process to the two faster components of the relaxation. The fact that A_F and A_S disappeared at approximately the same rate in the envelope test (Fig. 7) is additional evidence that A_F and A_S are linked together.

The argument that the two slower components remain after I_{Ca} has been 'washed out' (Byerly & Hagiwara, 1982) does not apply here. We have found Ca currents to be stable and large over periods of several hours following the initial 20–30 min of perfusion, provided the criteria we have outlined in the Methods section are observed (Brown, Wilson & Tsuda, 1983). There can be little doubt that internal perfusion is adequate, since Ca currents are not contaminated by outward currents at potentials below +50 mV, cardiac-type action potentials develop in normal extracellular solutions and direct measurements showed complete replacement of intracellular K and Cl ions (Akaike *et al.* 1978). There have been other reports of deterioration of Ca currents (Kostyuk, 1980; Fenwick *et al.* 1982) and the results have also been attributed to the loss of some specific cellular component. There is no direct evidence to support this interpretation and furthermore the 'wash out' phenomenon is not uniformly observed. In addition to the experiments reported at present, Caputo, DiPolo & Bezanilla (1983) found that Ca currents did not change in dialysed or perfused giant axons of squid, although K currents disappeared.

We have not been able to identify fully the current giving rise to A_{VS}. We have not identified a reversal potential; nor were we able to identify clear effects from changing $[Cs]_o$ (not shown). A_{VS} may arise from a channel which is completely non-specific and reverses at around 0 mV as suggested by Byerly & Hagiwara (1982), but we do not have compelling evidence for this. It appears to be distinguishable from I_{NS} by its very slow onset, its different potential dependence, and the fact that I_{NS} displays no significant tail current at −50 mV. The current does not seem to be a Ca-activated current, despite the fact that it is eliminated by Ca blockers, since its activation curve does not reflect the shape of the Ca I–V curve as normally observed for the Ca-activated K current (Meech, 1974). Furthermore, tail currents are similar for both Ba and Ca currents. We note that Ba does not activate K currents. This current also does not appear to be related to the Ca-activated leakage channels described by Colquhoun, Neher, Reuter & Stevens (1981) because of the differences in the voltage dependence of activation. Interestingly, the fact that we do not observe the A_{VS} component in some cells may be linked to our earlier observation (Brown

et al. 1981) that in some cells we observed a large I_{NS} that activates slowly, and in other cells we observed only a much smaller I_{NS} that activates rapidly. A_{VS} may be related to the very slow inward current observed in chromaffin cells (Fenwick *et al.* 1982).

In the envelope test we observed a decrease in the amplitude of the tail current that corresponded to the decay in the inward current during the pulse; this is good evidence that Ca current inactivates, and supports our earlier study of Ca current inactivation (Brown *et al.* 1981). Because the relaxation of the tail is bi-exponential and is independent of pulse length (Fig. 7), we may rule out contaminating currents which reverse at a potential other than V_H, such as the one which gives rise to A_{VS}. In addition, Cs, the major replacement ion in our experiments, would be expected to produce an outward current at -50 mV, since E_{Cs} is -80 mV in our experiments. We agree with Byerly & Hagiwara (1982) that the contaminating current giving rise to A_{VS} needs to be considered when one looks at the apparent inactivation of the Ca current. The following observation appears inconsistent with a large role in inactivation of the current that gives rise to A_{VS}. For a given depolarization, A_{VS} appears to be larger and activates faster in Ba than Ca. This seems incongruous with our earlier, consistent observation that I_{Ca} inactivates faster than I_{Ba}.

Ca channel currents

The results show that if we consider the time constants from both the turn-on and the turn-off of I_{Ca}, an m^2 model does not describe the activation process adequately. The main evidence against an m^2 model is that the ratio for the two tail τ's may be as great as 8:1 rather than the fixed 2:1 ratio predicted by the m^2 model. Additionally the time constant associated with the fastest component of the tail current relaxation is much too fast to reconcile with the τ_m obtained from a low-order Hodgkin–Huxley type description for turn-on at the same potential. Despite the very significant deviations from the latter type of model, it is interesting that we have made several observations which are consistent with measurements obtained from other voltage-dependent ionic currents. First, we have shown that the time course of the Ca current tail relaxations at a given recovery potential does not depend on the pulse height. Secondly, the amplitude of the tail relaxations seems to reflect the instantaneous current. This is shown by the fact that we constructed a reasonable I–V curve from an activation curve and an instantaneous I–V curve which were both obtained from tail current measurements. Thirdly, we observed that the time course of the tail relaxations did not change as a function of pulse length despite the fact that they were reduced due to inactivation. These observations are all consistent with a general formulation consisting of the product of an activation variable obtained from rate constants which depend only on potential, an inactivation variable, and an instantaneous I–V relation. There have, however, been two observations that indicate qualities of the Ca current which are perhaps unique. The striking effects of temperature on turn-on and not on turn-off are certainly unique observations. The observation of the small difference between Ca and Ba in terms of the turn-on and turn-off kinetics may also present a feature unique to the Ca current.

The present results may be compared with the recent results of Lux & Nagy (1981) and Brown *et al.* (1982) on single-channel Ca currents and Fenwick *et al.* (1982) for

unitary Ba currents. The observations of interest are the bursting of the discharge which often appears, and the fact that only one open state has been observed. This behaviour is consistent with a probabilistic interpretation of models such as we have considered here.

Our kinetic measurements appear to be consistent with a four-state model of activation rather than a three-state model as previously suggested (Fenwick *et al.* 1982). Fenwick *et al.* (1982), in their wide-ranging study which included measurements of tail currents, unitary activity and noise spectra, found comparable τ values among all three methods. They proposed a three-state sequential model to explain most but not all of their data. A three-state model was not sufficient for our results, as discussed at length previously. Briefly, for small depolarizations the delay in the onset, or turn-on, of I_{Ca} is simply too long to be accounted for by the fast relaxation shown by the tail currents at the same potential. Additionally, after cooling, turn-on was very much slowed at all potentials whereas τ_F and τ_S from the tail current measurements at -50 mV were changed very little. This indicates that turn-on must involve an exponential much different to those uncovered by turn-off at the holding potential. Hence, we have proposed a four-state model to explain our results, including the strikingly different effects of temperature on turn-on and turn-off. Interestingly the measurements and the model that we propose are similar to those described by Hahin & Goldman (1978*a*, *b*) for Na channels in *Myxicola* giant axon. These authors proposed a three-state model for Na activation and they found some discrepancy between the τ values measured from turn-on and turn-off. Perhaps a four-state model such as we have described may describe their data as well.

We can now re-examine the result of Kostyuk *et al.* (1981) in which a small step yielded a different τ_m value to that obtained from a larger step to the same potential. In the light of our present results, we have two points to make. First, with a model of activation such as we have described, the relaxation would be expected to be a sum of three exponentials, the relative amplitudes of each depending on the initial condition for the step. Thus for steps of varying size to the same potential there is no reason to expect the same τ values to be measured when one restricts the fit to one exponential. The second point has to do with the effect of temperature on the tail current. Kostyuk *et al.* (1981) performed their experiments at 10 °C, and their voltage protocols consisted of depolarizing voltage steps from rest to the test potential, V_t, followed by a small hyperpolarizing step and then a depolarizing step back to V_t. Since we have described the temperature effect on turn-on to be due to the leading forward rate constant, we would expect to see a much larger temperature effect on turn-on when starting with the channel population initially at rest as opposed to the effect observed when a significant number of channels are in states other than the resting state. Perhaps this is the reason that Kostyuk *et al.* (1981) measure a much larger time constant for turn-on due to a large step than for a small step. It would be interesting to repeat this experiment at a higher temperature.

As indicated in Fig. 6, the time constants of the bi-exponential tail relaxation decreased when the solution was changed from 5 to 20 mM-Ca. Similar results were obtained in another cell when Ca replaced Ba. Along with these effects there were smaller effects of the current-carrying species upon turn-on (not shown). Others have also found effects of the current-carrying species upon activation kinetics (Fenwick

et al. 1982; Saimi & Kung, 1982), although Byerly & Hagiwara (1982) and Kostyuk *et al.* (1981) have arrived at different conclusions. We wish to inject a note of caution that these results might be due to a small amount of the contaminating current that we found in most cells, as described earlier. For example, the difference between the tail τ values in going from Ca to Ba (Saimi & Kung, 1982) may simply be due to the shift in the activation curve of the contaminating component in going from Ba to Ca (Fig. 10*A* and *B*). Certainly in cells with a significant amount of the contaminating current (our A_{VS}), a very large effect on tail τ values could be seen using short pulses (Fig. 9*A*).

The instantaneous *I–V* reported here does not saturate as the return potential is hyperpolarized from +20 mV to the holding potential as reported previously (Kostyuk *et al.* 1981; Llinas *et al.* 1981). From Fig. 4 it is apparent that a probable reason for the discrepancy in the measurements may arise from using a preparation and voltage-clamp system in which the fastest component of the tail current relaxation is not resolved. The slower component does indeed show the saturation phenomena. This indicates that the strongly voltage-dependent binding site used by Llinas *et al.* (1981) to provide the saturation characteristic that they observed is not required to describe our data. Our instantaneous *I–V* data do, however, indicate a small deviation from the constant-field equation. Recall that the constructed peak *I–V* was obtained from the activation curve and the instantaneous *I–V* curve and that these were obtained from tail current measurements alone. The close fit of the constructed *I–V* to the measured *I–V* attests to the accuracy of our tail current measurements.

APPENDIX

Impedance measurements and the determination of R_S (work done in collaboration with H. M. Fishman)

Preliminary measurements of the impedance of the snail neurone were made in order to evaluate R_S. A diagram of the experimental arrangement is shown in Fig. 18. The measurements were conducted using a system developed by H. M. Fishman for making rapid transfer-function measurements. The system consists of a pseudo-random noise source (PS) and a spectrum analyser (Rockland 512/s) slaved to a LSI-11/23 microcomputer (Fishman, Poussart & Moore, 1979; Fishman, Moore & Poussart, 1981). There are several different Fourier synthesized PS wave forms stored in a read-only-memory (ROM), and this allows one to select a wave form which applies a spectral content such as to obtain good signal-to-noise characteristics at all frequencies in the output signal. Fourier transforms of the input and output were obtained on 1024 digitized points and 400 of the frequency domain points were displayed. A low-amplitude PS signal was applied to a 'current pump' circuit (Fishman, 1982) for passing current into the cell interior via the suction pipette. A low-impedance micro-electrode ($\sim$ 1 MΩ) with a driven shield for capacitance compensation was used as the voltage-sensing element. Current was collected from a silver–silver chloride pellet in the bath, and a current-to-voltage converter (*I–V*) circuit was used to measure the current.

The input signal for the measurement of the cell impedance was the current signal

derived from the $I-V$ converter. It should be pointed out that this signal was a true measure of the current through the cell whereas the PS signal was not correct due to capacitive shunting of the current from the current-pump circuit to ground via paths other than through the bath, as described below. The output signal for the measurement of the transfer function was the voltage in the cell interior. It was found

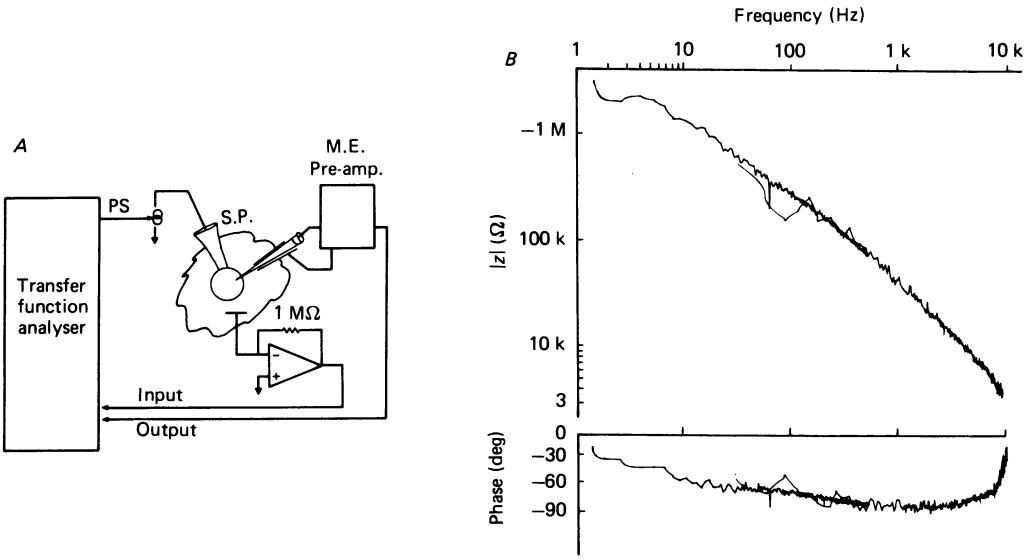

Fig. 18. Impedance measurement. *A*, diagram of the arrangement for measuring impedance. Current was applied from a current pump circuit to the cell via a suction pipette (S.P.) and voltage was measured with a shielded and compensated micro-electrode (M.E.). Current was collected from the bath, and the $I-V$ converter circuit was used to measure the current. The current signal from the $I-V$ converter and the voltage signal from the micro-electrode formed the input and output signals from which the 'transfer function analyser' obtained the impedance measurement. See text for further details. *B*, magnitude and phase of the impedance of a snail neurone. Corrections were applied as described in the text. The total frequency range displayed is from 1·25 Hz to 8 kHz and two measurements are shown with a region of overlap. The high-frequency asymptote of the impedance should reflect the series resistance of the cell. The phase and magnitude do not indicate a pure resistance; this indicates that the series resistance is less than the minimum impedance value shown here (5 kΩ). The phase lies between −60° and −80° over a wide range of frequencies, and the slope of the magnitude curve is slightly less than 20 dB/decade. This behaviour is indicative of a constant phase angle capacitance.

that two corrections were necessary to make the measurements in the above manner. First, the frequency response of the micro-electrode system was limited, and secondly, the $I-V$ converter presents an input impedance to ground which looks like an ideal inductor and which became significant at around 5–6 kHz. For each measurement, we thus obtained the current-to-voltage transfer function, and at each frequency value we did a complex division of this value by a value obtained from the measured micro-electrode transfer function. From this result to complex $I-V$ converter impedance was subtracted to obtain the cell impedance.

We evaluated certain components of our measurement system. The frequency response of the micro-electrode system was measured using the same system shown

in Fig. 15 with the exception that the cell was removed and a 500 kΩ resistor was placed between the pick-up electrode and the *I–V* converter. In this manner, the current signal may be simply scaled by the 500 kΩ resistor to obtain the voltage in the bath. It was found that with 1 MΩ micro-electrodes with carefully adjusted capacitance compensation one could obtain a magnitude response flat to as much as 10 kHz. We found that there was significant capacitive shunting of the suction pipette to ground via paths other than through the bath, as measured in the following manner. With the suction pipette in the bath, a current measurement obtained from the voltage drop across a resistor connecting the current-pump circuit to the suction pipette was compared to the current measurement from the *I–V* converter. There was a difference in these two measurements at high frequencies which appeared due to ~ 40 pF of capacitive shunting from the suction pipette apparatus to ground. Thus, all measurements were made using the bath electrode and the *I–V* converter. In addition to this measurement, we wished to evaluate the capacitive shunting through the suction pipette glass into the bath. This current component would circumvent the cell membrane but would be picked up by the bath electrode, and thus presented a possible source of error. This capacitive shunting was estimated by measuring the current in the bath when the suction pipette was driven from the current pump and the tip of the suction pipette was occluded. This measurement indicated a small capacitive component roughly estimated to be less than 3 pF. This value is much less than the cell capacitance and therefore should have negligible effects on the measurement.

The results are shown in Fig. 18 for a cell with the 'normal' intra- and extracellular solutions described in the Methods section. We expect the high frequency asymptote of the impedance to yield the series resistance of the cell. In our case at the highest frequency displayed, the impedance was not purely resistive; we thus estimate that R_S is some value which may be much less than 5 kΩ. Note that the phase lies between -60 and -85 degrees over a wide frequency range and the slope of the magnitude curve is slightly less than 20 dB/decade; this is characteristic of a constant phase-angle capacitance as has been measured in squid axon (Cole, 1976; Fishman, 1982). The slow relaxation noted by Byerly & Hagiwara (1982) can be explained by the constant phase angle and may be a general membrane property rather than the result of the membrane attached to the inner wall of the pipette as they have suggested. A comprehensive model of the cell impedance awaits further measurements and analyses, but for our purposes here we indicate that R_S is sufficiently small to produce negligible error in the voltage clamp (approximately 0·5 mV for a peak current of 100 nA and 1 mV during the measured tail current).

We thank Mr Bill Little for help with the computer programs, Mr Harold Henderson for help with the illustrations and Ms Dee Kelly for typing the manuscript. This work was done in partial fulfilment of a Ph.D. thesis of Mr D. L. Wilson and was supported by N.I.H. grants NS-11453 and HL-25145.

REFERENCES

ADAMS, D. J. & GAGE, P. W. (1977). Calcium channel in *Aplysia* nerve cell membrane: ionic and gating currents kinetics. *Proc. Aust. physiol. & pharmacol. Soc.* 8–28*P*.

ADAMSON, A. W. (1973). *A Textbook of Physical Chemistry*. New York: Academic Press.

AKAIKE, N., LEE, K. S. & BROWN, A. M. (1978). The calcium currents of *Helix* neuron. *J. gen. Physiol.* **71**, 509–532.

ARMSTRONG, C. M. (1981). Sodium channels and gating currents. *Physiol. Rev.* **61**, 644–683.

BEVINGTON, PHILIP R. (1969). *Data Reduction and Error Analysis for the Physical Sciences.* New York: McGraw-Hill.

BROWN, A. M., AKAIKE, N. & LEE, K. S. (1979). Reply to the letter on Kinetics of Calcium Inward Current Activation. *J. gen. Physiol.* **73**, 678–679.

BROWN, A. M., CAMERER, H., KUNZE, D. L. & LUX, H. D. (1982). Similarity of calcium current in three different species. *Nature, Lond.* **299**, 156–158.

BROWN, A. M., MORIMOTO, K., TSUDA, Y. & WILSON, D. (1981). Calcium current-dependent and voltage-dependent inactivation of calcium channels in *Helix aspersa*. *J. Physiol.* **320**, 193–218.

BROWN, A. M., WILSON, D. L. & TSUDA, Y. (1983). Perfusion of small excitable cells by glass pipette. *Intracellular Perfusion of Excitable Cells*, ed. KOSTYUK, P. G. & KRISHTAL, O. A. New York, London: John Wiley. (in the Press.)

BYERLY, L. & HAGIWARA, S. (1982). Calcium currents in internally perfused nerve cell bodies of *Limnea stagnalis*. *J. Physiol.* **322**, 503–528.

CAPUTO, C., DIPOLO, R. & BEZANILLA, F. (1983). Electrical recording of a voltage dependent Ca conductance in the squid axon. *Biophys. J.* **41**, 294a.

CHIU, S. Y. (1977). Inactivation of sodium channels: second order kinetics in myelinated nerve. *J. Physiol.* **273**, 573–596.

COLE, K. S. (1976). Electrical properties of the squid axon sheath. *Biophys. J.* **16**, 137–142.

COLQUHOUN, D. & HAWKES, A. G. (1977). Relaxation and fluctuations of membrane currents that flow through drug-operated channels. *Proc. R. Soc.* B **199**, 231–261.

COLQUHOUN, D., NEHER, E., REUTER, H. & STEVENS, C. F. (1981). Inward current channels activated by intracellular Ca in cultured cardiac cells. *Nature, Lond.* **294**, 752–754.

DEBOOR, CARL (1978). *A Practical Guide to Splines.* New York: Springer-Verlag.

EISENBERG, R. S. & ENGEL, E. (1970). The spatial variation of membrane potential near a small source of current in a spherical cell. *J. gen. Physiol.* **55**, 736–757.

FENWICK, E. M., MARTY, A. & NEHER, E. (1982). Sodium and calcium channels in bovine chromaffin cells. *J. Physiol.* **331**, 599–635.

FISHMAN, H. M. (1982). *Techniques in Cellular Physiology*, ed. BAKER, P. F., pp. 1–42. Amsterdam: Elsevier/North-Holland Scientific Publishers.

FISHMAN, H. M., MOORE, L. E. & POUSSART, D. (1981). Squid axon conduction: admittance and noise during short- *versus* long-duration step clamps. In *The Biophysical Approach to Excitable Membranes*, ed. ADELAMN, W. J., Jr & GOLDMAN, D. E., pp. 65–69. New York: Plenum.

FISHMAN, H. M., POUSSART, D. & MOORE, L. E. (1979). Complex admittance of Na conduction in squid axon. *J. Membrane Biol.* **50**, 43–53.

FITZHUGH, R. (1965). A kinetic model of the conductance changes in nerve membrane. *J. cell. comp. Physiol.* **66**, Suppl., 111–117.

HAGIWARA, S. & BYERLY, L. (1981). Calcium channel. *A. Rev. Neurosci.*, **4**, 69–125.

HAHIN, R. & GOLDMAN, L. (1978*a*). Initial conditions and the kinetics of the sodium conductance in *Myxicola* giant axons. I. Effects on the time-course of the sodium conductance. *J. gen. Physiol.* **72**, 863–877.

HAHIN, R. & GOLDMAN, L. (1978*b*). Initial conditions and the kinetics of the sodium conductance in *Myxicola* giant axons. II. Relaxation experiments. *J. gen. Physiol.* **72**, 879–898.

HODGKIN, A. L. & HUXLEY, A. F. (1952). A quantitative description of membrane current and its application to conduction and excitation in nerve. *J. Physiol.* **117**, 500–544.

KOSTYUK, P. G., KRISHTAL, O. A. & PIDOPLICHKO, V. I. (1977). Asymmetrical displacement currents in nerve cell membrane and effect of internal fluoride. *Nature, Lond.* **367**, 70–72.

KOSTYUK, P. G., KRISHTAL, O. A. & PIDOPLICHKO, V. I. (1981). Calcium inward current and related charge movements in the membrane of snail neurones. *J. Physiol.* **310**, 403–421.

KOSTYUK, P. G., KRISHTAL, O. A., PIDOPLICHKO, V. I. & SHAKHOVALOV, Y. A. (1979). Kinetics of Ca inward current activation. *J. gen. Physiol.* **73**, 675–677.

KOSTYUK, P. G. (1980). Calcium ionic channels in electrically excitable membrane. *Neuroscience* **5**, 945–959.

LEE, K. S., AKAIKE, N. & BROWN, A. M. (1980). The suction pipette method for internal perfusion and voltage clamp and small excitable cells. *J. neurosci. Methods* **2**, 51–78.

LLINAS, R., STEINBERG, I. Z. & WALTON, K. (1981). Presynaptic calcium currents in squid giant synapse. *Biophys. J.* **33**, 289–322.

LUX, H. D. & NAGY, K. (1981). Single channel Ca^{++} currents in *Helix potamia* neurons. *Pflügers Arch.* **391**, 252–254.

MEECH, R. W. (1974). The sensitivity of *Helix aspersa* neurons to injected calcium ions. *J. Physiol.* **237**, 259–277.

MORIMOTO, K., TSUDA, Y. & BROWN, A. M. (1981). Relative effectiveness of Ca channel blockers. *Fedn Proc.* **40**, 240.

SAIMI, Y. & KUNG, C. (1982). Are ions involved in the gating of calcium channels? *Science, N.Y.* **218**, 153–156.

SWISHER, G. M. (1976). *Introduction to Linear Systems Analysis.* Champaign, IL: Matrix.

THOMASSON, W. M. & CLARK, J. W. (1974). Analysis of exponential decay curves: a three step scheme for computing exponents. *Math. Biosci.* **22**, 179–195.

TSUDA, Y., WILSON, D. L. & BROWN, A. M. (1982*a*). Calcium tail currents in snail neurons. *Biophys. J.* **37**, 181a (abstract).

TSUDA, Y., WILSON, D. L. & BROWN, A. M. (1982*b*). Internal perfusion of small, excitable cells. In *Current Methods in Cellular Neurobiology*, ed. BARKER, J. & MCKELVY, J. New York: John Wiley. (in the Press.)

WILSON, D. L., MORIMOTO, K., TSUDA, Y. & BROWN, A. M. (1983). A quantitative analysis of surface charge effects on gating permeation of the calcium channel. *J. Membrane Biol.* **72**, 117–130.